abductor hallucis muscle after scalp stimulation and to onset of the action potential of the same muscle after lumbar stimulation were also measured, and the difference between the two latencies was estimated as central motor conduction time from the cortex to the lumbar segment of the spinal cord (L-CMCT). The C-CMCT for the right thenar muscle was 9.4 ms (normal: up to 10 ms). The L-CMCT for the abductor hallucis muscle was 15.8 ms, showing a slight increase (normal: up to 15 ms). On spirometry, forced vital capacity (FVC) was 1.87 L, % predicted value (%VC) was 59.8%, and forced expiratory volume (FEV) 1.0% was 81.7%, showing restrictive ventilation dysfunction. There were no abnormalities in cerebrospinal fluid, which tested negative for type I poliovirus antibodies. CT showed diffuse severe muscular atrophy and fatty degeneration from the right hip through the entire leg (Fig. 1A and B). Atrophy of the paraspinal and intercostal muscles was also seen. Brain MRI showed mild atrophy, but no abnormal signals were seen along the corticospinal tract.

Two months after admission he required non-invasive positive pressure ventilation by nasal mask for his sleep disorder. After 4 months he could not orally ingest food sufficiently because of his breathing difficulty. After 5 months his pulmonary function showed an FVC of 0.99 L, %VC of 38.1%, and FEV 1.0% of 41.3%. In arterial blood gas analysis (room air), both PaO_2 and $PaCO_2$ continued to be about 60 Torr. After 6 months the patient died from respiratory failure. The clinical diagnosis was a residue of paralytic polio and ALS presenting as respiratory failure. An autopsy was performed about 8 h after death.

Brain weight was 1370 g. No marked changes were seen in the brain grossly, but there was atrophy of the spinal ventral roots. Histologically, motor neuron loss in the spinal ventral horn was seen. In the anterior horn of the left lumbar cord, active degeneration was seen, including atrophied motor neurons with Bunina bodies, appearance of macrophages, axonal spheroids, and hypertrophic astrocytes (Figs. 2–4). On the right side, atrophy of the ventral horn, extensive neuronal loss, and gliosis were seen, but there were few findings of active degeneration (Fig. 3). At the cervical and thoracic levels, there was not a clear difference between motor neuron lesions on the right and left sides. Mild cell loss in the hypoglossal nuclei was present. Bunina bodies were also seen in remaining motor neurons of the cervical anterior horn and the hypoglossal nuclei. There was mild loss of Betz cells in the motor cortex. In the spinal cord, the lateral column demonstrated a slight pallor bilaterally with Klüver–Barrera stain (Fig. 2), and the presence of macrophages. Glial bundles were seen on the right side, particularly in the lumbar ventral roots. Neurogenic atrophy was also seen in the intercostal muscles and diaphragm.

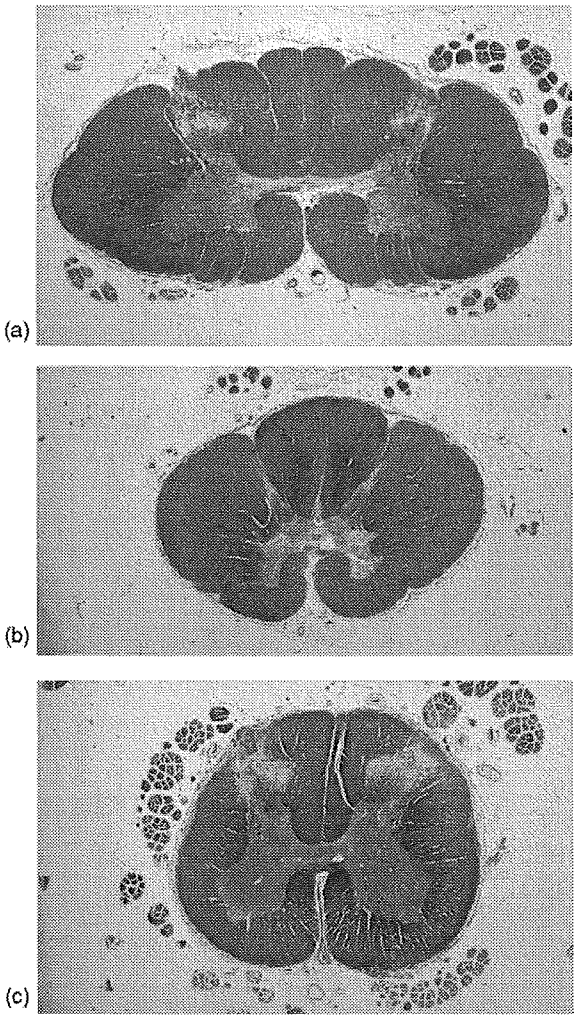

Fig. 2. Spinal cord findings. Transverse section at the spinal level ((a) cervical, (b) thoracic, and (c) lumbar). Mild pallor is seen in the lateral columns at the lumbar level. Klüver–Barrera stain (×3).

3. Discussion

The present patient had a history of paralytic polio in childhood. After a stable period of about 65 years, he suffered severe weight loss and a respiratory disorder. This was a rare case in which the lower motor neuron symptoms and signs were in the foreground, and the condition rapidly progressed to fatal respiratory failure. The findings included some atypical features for ALS, namely, absence of the obvious clinical pyramidal signs.

Typical symptoms of PPS and PPMA include new deterioration of muscle strength, general fatigue, speech and vocal impairment, dysphagia, and depression.

Rather than a reinfection or reactivation of the poliovirus or a new progressive degenerative process, PPS may be a secondary functional disorder from the addition of age-related changes to existing functional failure [7–10]. Among PPS cases, progressive ventilation failure such as chronic alveolar hypoventilation, progressive respiratory failure, and sleep apnea syndrome have been reported [18,19]. The clinicopathological diagnosis of our patient was more likely ALS presenting as respiratory failure or dyspnea-fasciculation syndrome [20], rather than respiratory disorder due to PPS or PPMA.

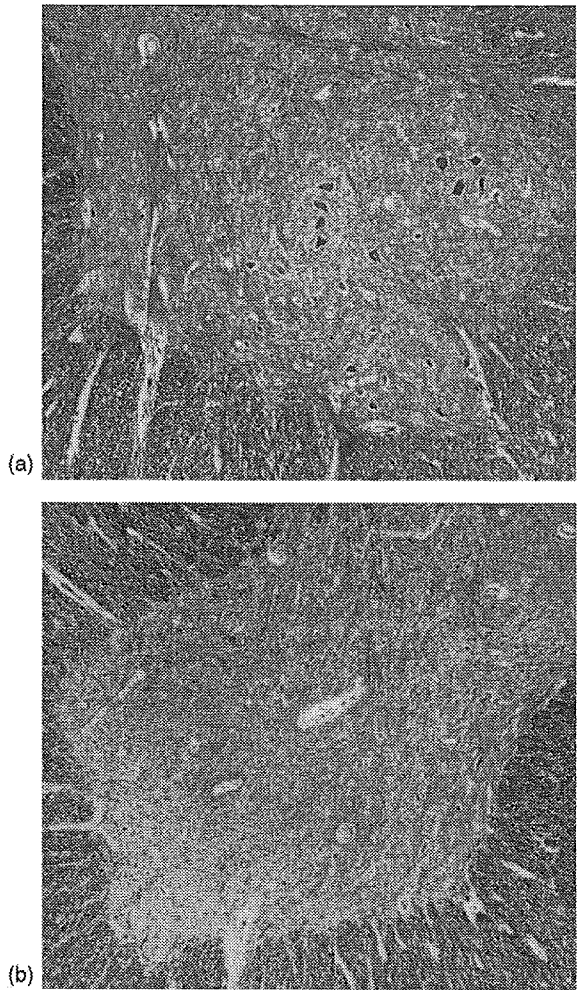

Fig. 3. Spinal ventral horn findings. Transverse sections of the lumbar ventral horn. Mild to moderate loss of motor neurons is seen on the left side (a). On the right side (b), ventral horn atrophy, severe motor neuron loss, and gliosis are seen. Klüver–Barrera stain (×10).

Recently, Truffert et al. [21] have reported that a 56-year-old man with prior paralytic poliomyelitis developed progressive respiratory failure caused by endplate dysfunction. Repetitive stimulation studies showed a marked decrement of the trapezius muscle response, which was reversible with edrophonium. In the absence of biological evidence for autoimmune myasthenia gravis, it may be that some kind of endplate dysfunction mechanism is related to postpolio syndrome. The repetitive stimulation procedure should be considered in postpolio syndrome patients as some of them may benefit from anticholineesterase treatment. In our patient the negative result from the edrophonium test was rather unsuggestive of significant endplate dysfunction. Truffert et al. reported a patient whose presentation was quite similar to the present case, but who improved with anticholinesterase therapy, contrary to our patient.

Neuropathological reports on ALS patients with antecedent paralytic polio are rare. Roos et al. [12] reported an ALS patient who had contracted poliomyelitis at the age of 15 years. This patient had weakness of the right hand at the age of 45, and died 3 years later. These authors noted that, neuropathologically, this case presented a classical picture of ALS. Shimada et al. [13] reported a woman who had leg paralysis from acute poliomyelitis at the age of 2 years, onset of progressive weakness of the left hand at the age of 75, and respiratory failure causing death at the age of 80.

Neuropathologically, there were findings of old poliomyelitis in the lumbar ventral horn, together with ALS pathology presenting cortical and spinal motor neuron damage. However, they described several atypical findings that differed from classical ALS [22], including the preservation of the hypoglossal nucleus, no Bunina bodies in the remaining motor neurons, and no ubiquitin-positive inclusions. Pezeshkpour et al. [23] reported local, asymmetric spinal anterior horn motor neuron degeneration and a well-preserved corticospinal tract. Miller [24] indicated that PPMA patients presented spinal motor neuron loss and axon spheroids, and mild spinal lateral funiculus damage and loss of Betz cells in the motor cortex.

In the present case, there was atrophy in the right lumbar anterior horn, and severe loss of cells of all sizes, from large alpha motor neurons to small interneurons. This was quite different from the size-dependent selective pattern of

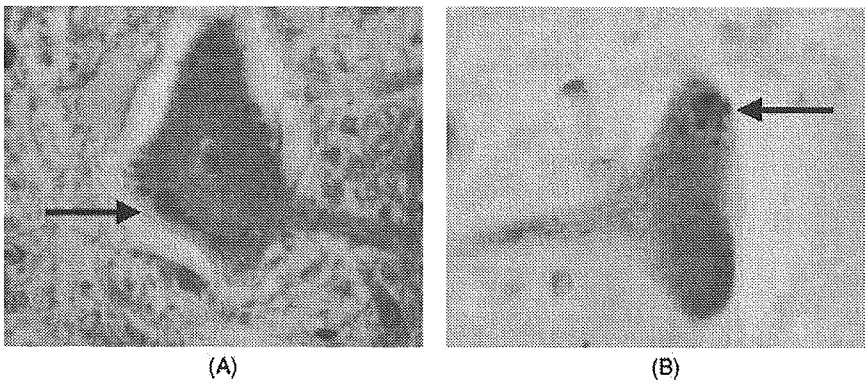

Fig. 4. Bunina body findings. (A) Shows Bunina bodies (arrows) in motor neurons of the lumbar ventral horn with hematoxylin-eosin stain (×100). (B) Shows cystacin-C stain (×100).

motor neuron loss in ALS [25–28]. The glial bundles present predominantly in the right lumbar spinal roots were those from paralytic polio [29]. Otherwise, the pathophysiological findings were indistinguishable from those of sporadic ALS. The extremely rapid progression of motor neuron dysfunction resulting in respiratory failure may reflect the underlying dormant pathophysiological process due to antecedent poliovirus infection, since antecedent poliovirus infection would have spread far beyond the lesions of apparent motor neuron loss [18,19].

In patients with a history of paralytic poliomyelitis who present progressive respiratory failure after a long and stable course, one may consider not only respiratory disorder due to PPS but also, in rare cases, the development of ALS.

References

[1] Bonduelle M. Amyotrophic lateral sclerosis. In: Vinken PJ, Bruyn GW, editors. System disorders and atrophies. Part II. Handbook of clinical neurology, vol. 22. Amsterdam: North-Holland Publishing Co.; 1975. p. 281–338.
[2] Hughes JT. Pathology of amyotrophic lateral sclerosis. Adv Neurol 1982;36:61–74.
[3] Leigh PN, Ray-Chaudhuri K. Motor neuron disease. J Neurol Neurosurg Psychiatry 1994;57:886–96.
[4] Pouget J, Azulay J-P, Bille-Turc F, Sangla I, Serratrice GT. The diagnosis of amyotrophic lateral sclerosis. Adv Neurol 1995;68:143–52.
[5] Traynor BJ, Codd BM, Corr B, Forde C, Frost E, Hardiman OM. Clinical features of amyotrophic lateral sclerosis according to the El Escorial and Airlie House Diagnostic Criteria. Arch Neurol 2000;57:1171–6.
[6] Lyall RA, Donaldson N, Polkey MI, Leigh PN, Moxham J. Respiratory muscle strength and ventilatory failure in amyotrophic lateral sclerosis. Brain 2001;124:2000–13.
[7] Dalakas MC, Elder GE, Hallett M, Ravits J, Baker M, Papadopoulos N, et al. A long-term follow-up study of patients with post-poliomyelitis neuromuscular symptoms. N Engl J Med 1986;314:959–63.
[8] Dalakas MC, Ilia I. Post-polio syndrome: concepts in clinical diagnosis, pathogenesis, and etiology. Adv Neurol 1991;56:495–511.
[9] Dalakas MC. The post-polio syndrome as an evoked clinical entity definition and clinical description. Ann NY Acad Sci 1995;753:68–80.
[10] Halstead LS. Diagnosing postpolio syndrome: inclusion and exclusion criteria. In: Silver JK, Gawne AC, editors. Postpolio syndrome. Philadelphia: Hanley & Belfus; 2004. p. 1–20.
[11] Mulder DW, Rosenbaum RA, Layton DD. Late progression of poliomyelitis or forme fruste amyotrophhic lateral sclerosis? Mayo Clin Proc 1972;47:756–61.
[12] Roos RP, Viola MV, Wollmann R, Hatch MH, Antel JP. Amyotrophic lateral sclerosis with antecedent poliomyelitis. Arch Neurol 1980;37:312–3.
[13] Shimada A, Lange DJ, Hays AP. Amyotrophic lateral sclerosis in an adult following acute paralytic poliomyelitis in early childhood. Acta Neuropathol 1999;97:317–21.
[14] Norris FH, Denys EH, Sang UK. Polio and ALS. Neurology 1990;40:1150.
[15] Armon C, Daube JR, Windebank AJ, Kurland LT. How frequently does classic amyotrophic lateral sclerosis develop in survivors of poliomyelitis? Neurology 1990;40:172–4.
[16] Moriwaka F, Tashiro K, Okumura H, Yamada T. ALS and poliomyelitis. Neurology 1991;41:612.
[17] Okumura H, Kurland LT, Waring SC. Amyotrophic lateral sclerosis and polio: Is there an association? Ann NY Acad Sci 1995;753:245–56.
[18] Dean E, Ross J, Road JD, Courtenay L, Madill KJ. Pulmonary function in individuals with a history of poliomyelitis. Chest 1991;100:118–23.
[19] Mahgoub A, Cohen R, Rossoff LJ. Weakness, daytime somnolence, cough, and respiratory distress in a 77-year-old man with a history of childhood polio. Chest 2001;120:659–61.
[20] Scelsa SN, Yakubov B, Salzman SH. Dyspnea-fasciculation syndrome: early respiratory failure in ALS with minimal motor signs. Amyotroph Lateral Scler Other Motor Neuron Disord 2002;3:239–43.
[21] Truffert A, Lalive PH, Janssens JP, Sinnreich M, Magistris MR. Endplate dysfunction causing respiratory failure in a patient with prior paralytic poliomyelitis. J Neurol Neurosurg Psychiatry 2003;74:370–2.
[22] Ito H, Hirano A. Comparative study of spinal cord ubiquitin expression in post-poliomyelitis and sporadic amyotrophic lateral sclerosis. Acta Neuropathol 1994;87:425–9.
[23] Pezeshkpour GH, Dalakas MC. Long-term changes in the spinal cords of patients with old poliomyelitis: signs of continuous disease activity. Arch Neurol 1988;45:505–8.
[24] Miller DC. Post-polio syndrome spinal cord pathology: case report with immunopathology. Ann NY Acad Sci 1995;753:186–93.
[25] Terao S, Sobue G, Hashizume Y, Mitsuma T, Takahashi A. Disease specific patterns of neuronal loss in the spinal ventral horn in amyotrophic lateral sclerosis, multiple system atrophy and X-linked recessive bulbospinal neuronopathy; with special reference to the loss of small-sized neuron in the intermediate zone. J Neurol 1994;241:196–203.
[26] Terao S, Li M, Hashizume Y, Osano Y, Mitsuma T, Sobue G. Upper motor neuron lesions in stroke patients do not induce anterograde transneuronal degeneration in spinal anterior horn cells. Stroke 1997;28:2553–6.
[27] Terao S, Sobue G, Li M, Hashizume Y, Tanaka F, Mitsuma T. The lateral corticospinal tract and spinal ventral horn in X-linked recessive spinal and bulbar muscular atrophy: a quantitative study. Acta Neuropathol 1997;93:1–6.
[28] Terao S, Li M, Hashizume Y, Mitsuma T, Sobue G. No transneuronal degeneration between human cortical motor neurons and spinal motor neurons. J Neurol 1999;246:61–2.
[29] Iwata M, Hirano A. "Glial bundles" in the spinal cord late after paralytic anterior poliomyelitis. Ann Neurol 1978;4:562–3.

nature medicine

17-AAG, an Hsp90 inhibitor, ameliorates polyglutamine-mediated motor neuron degeneration

Masahiro Waza[1,2], Hiroaki Adachi[1,2], Masahisa Katsuno[1], Makoto Minamiyama[1], Chen Sang[1], Fumiaki Tanaka[1], Akira Inukai[1], Manabu Doyu[1] & Gen Sobue[1]

Heat-shock protein 90 (Hsp90) functions as part of a multichaperone complex that folds, activates and assembles its client proteins. Androgen receptor (AR), a pathogenic gene product in spinal and bulbar muscular atrophy (SBMA), is one of the Hsp90 client proteins. We examined the therapeutic effects of 17-allylamino-17-demethoxygeldanamycin (17-AAG), a potent Hsp90 inhibitor, and its ability to degrade polyglutamine-expanded mutant AR. Administration of 17-AAG markedly ameliorated motor impairments in the SBMA transgenic mouse model without detectable toxicity, by reducing amounts of monomeric and aggregated mutant AR. The mutant AR showed a higher affinity for Hsp90-p23 and preferentially formed an Hsp90 chaperone complex as compared to wild-type AR; mutant AR was preferentially degraded in the presence of 17-AAG in both cells and transgenic mice as compared to wild-type AR. 17-AAG also mildly induced Hsp70 and Hsp40. 17-AAG would thus provide a new therapeutic approach to SBMA and probably to other related neurodegenerative diseases.

Hsp90, which accounts for 1–2% of cytosolic protein, is one of the most abundant cellular chaperone proteins[1]. It functions in a multicomponent complex of chaperone proteins including Hsp70, Hop (Hsp70 and Hsp90 organizing protein), Cdc37, Hsp40 and p23. Hsp90 is involved in the folding, activation and assembly of several proteins, known as Hsp90 client proteins[1]. As numerous oncoproteins have been shown to be Hsp90 client proteins[1], Hsp90 inhibitors have become a new strategy in antitumor therapy[2]. Geldanamycin, a classical Hsp90 inhibitor, is known as a potent antitumor agent[2]; however, it has not been used in clinical trials because of its liver toxicity[3]. 17-AAG is a new derivative of geldanamycin that shares its important biological activities[4] but shows less toxicity[5].

Hsp90 requires several interacting, co-chaperone proteins to exert its function on Hsp90 client proteins in Hsp90 complexes[1], of which two main forms exist[6]. One complex is a proteasome-targeting form associated with Hsp70 and Hop, and the other is a stabilizing form with Cdc37 and p23 (refs. 7,8). Particularly, p23 is thought to modulate Hsp90 activity in the last stages of the chaperoning pathway, leading to stabilized Hsp90 client proteins[9]. Hsp90 inhibitors, including 17-AAG, inhibit the progression of the Hsp90 complex toward the stabilizing form[10–12], and shift it to the proteasome-targeting form[7,8], resulting in enhanced proteasomal degradation of the Hsp90 client protein[7,13–18].

Because 17-AAG has less toxicity and higher selectivity for client oncoproteins[19], 17-AAG is now in clinical trials for a wide range of malignancies[20]. Additionally, Hsp90 inhibitors also function as Hsp inducers[20,21]. Several previous studies have suggested that Hsp90 inhibitors could be applied to nononcological diseases as neuroprotective agents based on their induction of Hsps[22–28].

Androgen receptor (AR) is one of the Hsp90 client proteins[15], and is a pathogenic gene product of spinal and bulbar muscular atrophy (SBMA), one of the polyglutamine (polyQ) diseases[29]. This disease is characterized by premature muscular exhaustion, slow progressive muscular weakness, atrophy and fasciculation in bulbar and limb muscles[30]. PolyQ diseases are inherited neurodegenerative disorders caused by the expansion of a trinucleotide CAG repeat in the causative genes[31]. In SBMA, the number of polymorphic CAG repeats is normally 14–32, whereas it is expanded to 40–62 CAGs in the *AR* gene[32]. A correlation exists between CAG repeat size and disease severity[33]. The pathologic features of SBMA are motor neuron loss in the spinal cord and brainstem[30], and diffuse nuclear accumulation and nuclear inclusions of the mutant AR in the residual motor neurons and certain visceral organs[34].

We have already examined several therapeutic approaches in a mouse model of SBMA[35–38]. As a consequence, we confirmed that castration and leuprorelin, a luteinizing hormone–releasing hormone agonist that reduces testosterone release from the testis, substantially rescued motor dysfunction and nuclear accumulation of mutant AR in male transgenic mice[35,37]. Although this hormonal therapy was effective, it poses the unavoidable difficulty of severe sexual dysfunction[37]. In addition, this therapy cannot be applied to other polyQ diseases.

Here, we present a new and potent strategy for SBMA therapy with 17-AAG, an Hsp90 inhibitor. Given that Hsp90 inhibitors have two major activities, preferential client protein degradation and Hsp induction, we hypothesized that 17-AAG would degrade mutant AR more effectively than wild-type AR.

[1]Department of Neurology, Nagoya University Graduate School of Medicine, 65 Tsurumai-cho, Showa-ku, Nagoya 466-8550, Japan. [2]These authors contributed equally to this work. Correspondence should be addressed to G.S. (sobueg@med.nagoya-u.ac.jp).

Received 25 February; accepted 10 August; published online 11 September 2005; doi:10.1038/nm1298

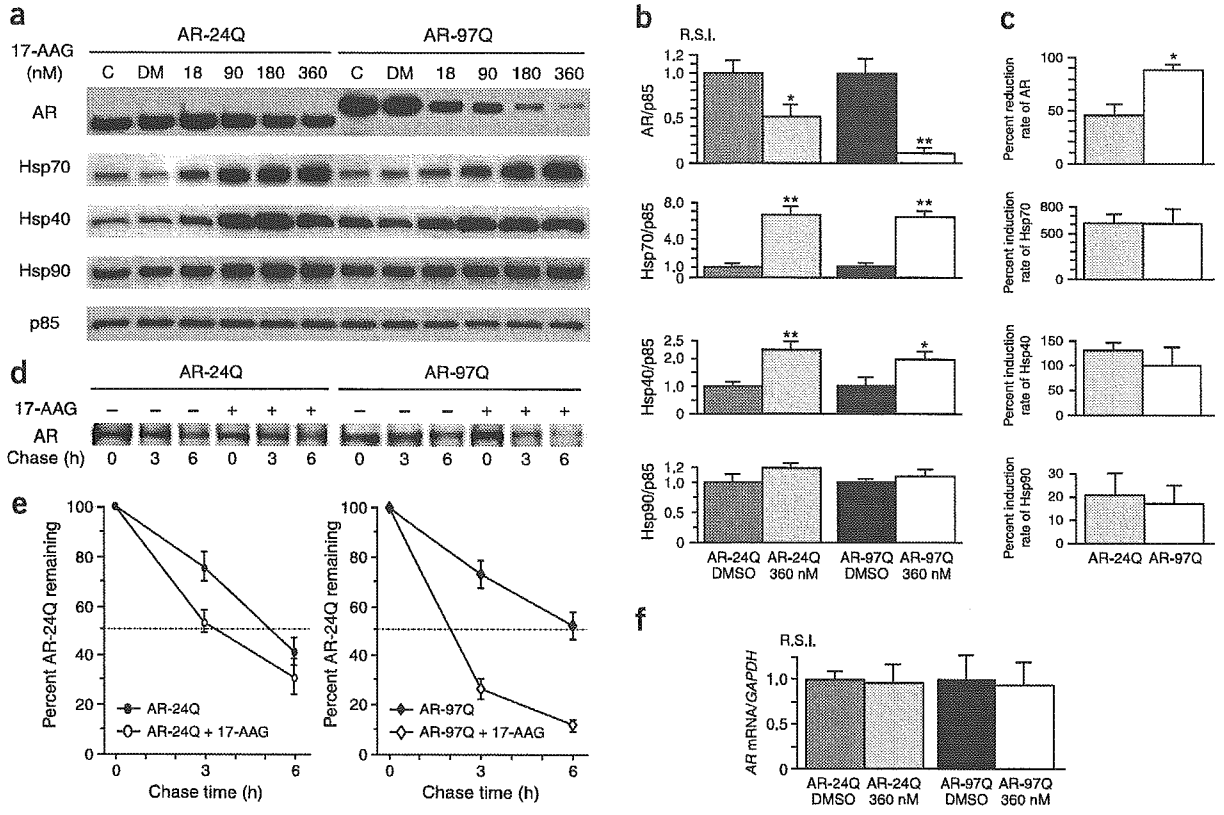

Figure 1 Effect of 17-AAG on the AR or chaperones in cultured-cell models. (**a**,**b**) Although the immunoblot and densitometric analysis showed a dose-dependent decline in both wild-type (AR-24Q) and mutant (AR-97Q) AR expression in response to 17-AAG, the mutant AR decreased more than did the wild-type. 17-AAG markedly increased the expression of Hsp70 and Hsp40, especially for Hsp70, but only slightly increased Hsp90 expression. (**c**) The decrease in mutant AR after treatment with 17-AAG was much higher than that of wild-type AR (88.9% versus 45.9%, $P = 0.0063$). Values are expressed as mean ± s.e.m. ($n = 5$). (**d**) Pulse-chase analysis of two forms of AR. Data from one representative experiment for wild-type and mutant AR. (**e**) Pulse-chase assessment of the half-life of wild-type and mutant AR. The amounts of AR-24Q and AR-97Q remaining in the absence and presence of 17-AAG are indicated. Values are expressed as mean ± s.e.m. ($n = 4$). (**f**) Real-time RT-PCR of wild-type and mutant *AR* mRNA. Quantities are shown as the ratio to *GAPDH* mRNA. The wild-type and mutant *AR* mRNA levels were similar under 17-AAG treatments. Values are expressed as mean ± s.e.m. ($n = 4$). $^*P < 0.025$, $^*P < 0.005$.

In this study, we examine the effects of 17-AAG on a cultured-cell model and the transgenic mouse model of SBMA. We show that the mutant AR exists more frequently as a stabilized Hsp90 chaperone complex than does the wild-type AR, and that 17-AAG selectively degrades the mutant AR. Administration of 17-AAG inhibits neuronal nuclear accumulation of the mutant AR and considerably ameliorates motor phenotypes of the SBMA model mouse.

RESULTS

Effect of 17-AAG on expression of AR and Hsps *in vitro*

To address the question of whether 17-AAG promotes the degradation of polyQ-expanded AR, we treated SH-SY5Y cells highly expressing the wild-type (AR-24Q) or mutant (AR-97Q) AR for 48 h with the indicated doses of 17-AAG or with DMSO as control. Although immunoblot analysis showed a dose-dependent decline in both wild-type and mutant AR expression after treatment with 17-AAG (**Fig. 1a**), the monomeric mutant AR decreased significantly more than did the wild-type ($P = 0.0063$; **Fig. 1b,c**), suggesting that the mutant AR is more sensitive to 17-AAG than is the wild-type. The expression of Hsp70 and Hsp40 were also markedly increased after treatment with 17-AAG, but Hsp90 was only slightly increased (**Fig. 1a,b**). There were no significant differences, however, in the levels of Hsp70, Hsp40 and Hsp90 induction between the wild-type and mutant AR (**Fig. 1c**).

To determine whether the decrease in AR resulted from protein degradation or from changes in RNA expression, we assessed the turnover of wild-type and mutant AR with a pulse-chase labeling assay. Without treatment, the wild-type and mutant AR were degraded in a similar manner, as previously reported[39,40]. In the presence of 17-AAG, however, the wild-type and mutant AR had half-lives of 3.5 h and 2 h, respectively (**Fig. 1d,e**), whereas levels of mRNA encoding the wild-type and mutant AR were quite similar (**Fig. 1f**). Cell viability did not differ between wild-type and mutant AR transfected cells (data not shown). These data indicate that 17-AAG preferentially degrades the mutant AR protein without cellular toxicity or alteration of mRNA levels.

To address why 17-AAG preferentially degrades mutant AR, we determined the levels of Hsp90, Hop and p23 associated with wild-type or mutant AR in SH-SY5Y cells without 17-AAG treatment (**Fig. 2a**). Hop and p23 are two essential components of multi-chaperone Hsp90 complexes[1]. Without 17-AAG treatment, coimmunoprecipitation from the cell lysates with antibodies to AR showed that p23 was more highly associated with mutant than with wild-type AR (**Fig. 2a,b**). The total levels of Hsp90, Hop and p23 were similar in the cells transfected with either wild-type or mutant AR (**Fig. 2a**).

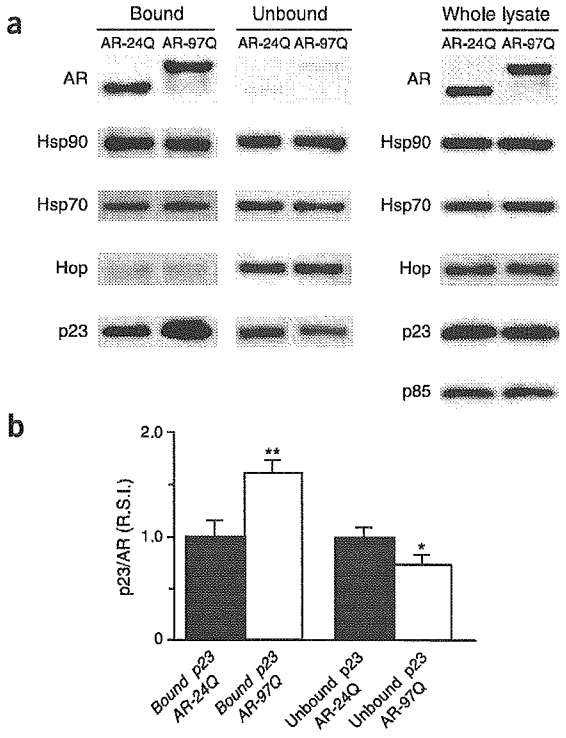

Figure 2 Immunoprecipitation of wild-type and mutant AR in cultured-cell models. (**a**) Wild-type and mutant AR were immunoprecipitated from cell lysates with an AR-specific antibody and immunoblotted with antibodies to the indicated western blot proteins. There was more mutant AR present in multichaperone complexes with p23 than there was wild-type AR. There were no differences in total expression levels of AR, Hsp90, Hsp70, Hop and p23 between wild-type and mutant AR–expressing cells. Control immunoprecipitations without antibodies did not immunoprecipitate any co-chaperones (data not shown). (**b**) The densitometric analysis of p23 in the bound and unbound fractions shows there was 1.6 times as much p23 associated with mutant AR than there was with the wild-type ($P < 0.01$). This experiment was repeated with five sets of cells with equivalent results. Values are expressed as mean ± s.e.m. ($n = 5$). $^*P < 0.05$, $^{**}P < 0.01$. R.S.I., relative signal intensity.

We next examined the status of the Hsp90 chaperone complex in wild-type and mutant AR-expressing cultured cells treated with 17-AAG. Immunoprecipitation with AR-specific antibody showed that Hsp90 chaperone complex–associated Hop was markedly increased, and p23 decreased depending on the dose of 17-AAG (**Fig. 3a,b**), suggesting that treatment with 17-AAG resulted in the shifting of the AR-Hsp90 chaperone complex from a mature stabilizing form with p23 to a proteasome-targeting form with Hop. The loss of p23 from the mutant AR-Hsp90 complex was significantly higher ($P < 0.005$) than that from the wild-type AR-Hsp90 complex (**Fig. 3c**). The degradation of wild-type and mutant AR by 17-AAG was completely blocked by the proteasome inhibitor MG132 (**Fig. 3d**), suggesting that the pharmacological degradation by 17-AAG was dependent on the proteasome system, as previously reported[17,18]. Furthermore, these results strongly suggest that mutant AR is more likely to be in the Hsp90-p23 multichaperone complexes, which eventually enhances 17-AAG–dependent proteasomal degradation of mutant AR.

Moreover, mutant AR was markedly decreased after treatment with 17-AAG even when induction of Hsp70 and Hsp40 was blocked by the protein-synthesis inhibitor cycloheximide (**Supplementary Fig. 1** online), suggesting that 17-AAG contributes to the preferential degradation of mutant AR mainly through Hsp90 chaperone complex formation and subsequent proteasome-dependent degradation rather than through induction of Hsp70 and Hsp40.

17-AAG ameliorates phenotypic expression of SBMA mice

We administered 17-AAG (2.5 or 25 mg/kg) to male transgenic mice carrying full-length human AR-24Q or AR-97Q. The disease progression of AR-97Q mice treated with 25 mg/kg 17-AAG (Tg-25) was

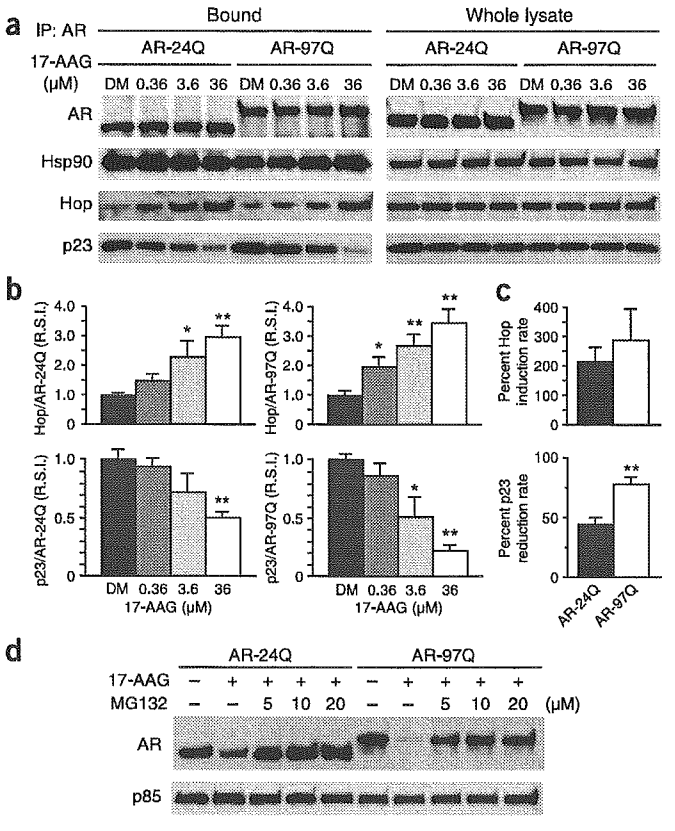

Figure 3 Pharmacological change in the AR-Hsp90 complex, and the correlation to proteasomal degradation. (**a**) Immunoblots of lysates of transfected cells treated with 17-AAG. Lysates were immunoprecipitated with AR-specific antibody. The short time exposure to 17-AAG did not decrease the amount of mutant AR. There were dose-dependent changes in both Hop and p23 after treatment with 17-AAG; however, no dissociation of Hsp90 from the mutant AR complex was seen. There were no changes in the expression of Hop, p23 and Hsp90 in whole lysates in the presence of 17-AAG. (**b**) Densitometric analysis of Hop and p23 in the bound fractions. There was a marked increase in the amount of Hop, and a marked decrease in p23 in both wild-type and mutant AR-bound Hsp90 complexes after treatment with 17-AAG. R.S.I., relative signal intensity. (**c**) Comparisons of induction rate of Hop and reduction rate of p23 in the Hsp90 complexes of wild-type and mutant AR. Although there was no significant difference in the induction rate of Hop between the wild-type and mutant AR complexes, the reduction rate of p23 was significantly higher in the mutant AR complex compared with that in the wild-type complex (43.8% versus 79.0%, $P < 0.005$). Values are expressed as means ± s.e.m. ($n = 5$). (**d**) Effect of 17-AAG on AR expression under the inhibition of proteasomal degradation. The mutant AR was more markedly reduced than wild-type AR after 17-AAG treatments; however, this pharmacological degradation was completely blocked by MG132 in both cases. DM, DMSO. $^*P < 0.025$, $^*P < 0.005$.

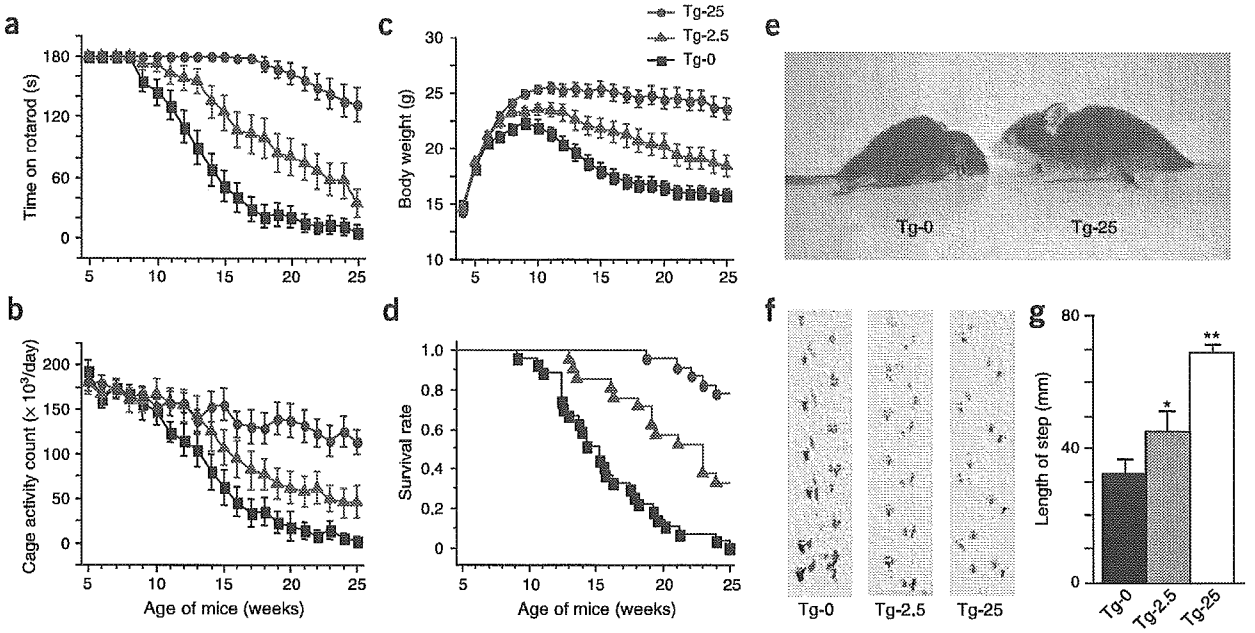

Figure 4 Effects of 17-AAG on behavioral and visible phenotypes in male AR-97Q mice. (**a**) Rotarod task ($n = 27$), (**b**) cage activity ($n = 18$), (**c**) body weight ($n = 27$) and (**d**) survival rate ($n = 27$) of Tg-0, Tg-2.5 and Tg-25 mice. All parameters were significantly different between the Tg-0 and Tg-25 ($P < 0.005$ for all parameters). A Kaplan-Meier plot shows the prolonged survival of Tg-2.5 and Tg-25 compared with Tg-0, which had all died by 25 weeks of age ($P = 0.004$, $P < 0.001$, respectively). (**e**) Representative photographs of a 16-week-old Tg-0 (left) shows an obvious difference in size, and illustrates muscular atrophy and kyphosis compared with an age-matched Tg-25 (right). (**f**) Footprints of representative 16-week-old Tg-0, Tg-2.5 and Tg-25 mice. Front paws are indicated in red and hind paws in blue. (**g**) The length of steps was measured in 16-week-old Tg-0, Tg-2.5 and Tg-25 mice. Each column shows an average of steps of the hind paw. Values are expressed as means ± s.e.m. ($n = 6$). $^*P < 0.025$, $^{**}P < 0.005$.

markedly ameliorated, and that of mice treated with the 2.5 mg/kg 17-AAG (Tg-2.5) was mildly ameliorated (**Fig. 4a–d**). The untreated transgenic male mice (Tg-0) showed motor impairment assessed by the rotarod task as early as 9 weeks after birth, whereas Tg-25 mice showed initial impairment only 18 weeks after birth and with less deterioration than Tg-0 mice (**Fig. 4a**). Tg-2.5 mice showed intermediate levels of impairment in rotarod performance (**Fig. 4a**). The locomotor cage activity of Tg-0 mice was also markedly decreased at 10 weeks compared with the other two groups, which showed decreases in activity at 13 (Tg-2.5) and 16 (Tg-25) weeks of age (**Fig. 4b**). Tg-0 mice lost weight significantly earlier and more profoundly than the Tg-2.5 ($P < 0.025$) and Tg-25 mice ($P < 0.005$; **Fig. 4c**). Treatment with 17-AAG also significantly prolonged the survival rate of Tg-2.5 ($P = 0.004$) and Tg-25 mice ($P < 0.001$) as compared to Tg-0 mice (**Fig. 4d**). 17-AAG was less effective at the close of 2.5 mg/kg than 25 mg/kg in all parameters tested. The lines were not distinguishable in terms of body weight at birth; however, by 16 weeks, Tg-0 mice showed obvious differences in body size, muscular atrophy and kyphosis compared to Tg-25 mice (**Fig. 4e**). Additionally, Tg-0 mice showed motor weakness, with short steps and dragging of the legs, whereas Tg-25 mice showed almost normal ambulation (**Fig. 4f,g**).

When we immunohistochemically examined mouse tissues for mutant AR using the 1C2 antibody, which specifically recognizes expanded polyQ, we observed a marked reduction in 1C2-positve nuclear accumulation in the spinal motor neurons (**Fig. 5a**) and muscles (**Fig. 5b**) of Tg-25 mice compared with those of Tg-0 mice. Glial fibrillary acidic protein (GFAP)-specific antibody staining showed an apparent reduction of reactive astrogliosis in Tg-25 compared with Tg-0 mice in the spinal anterior horn (**Fig. 5c**). Muscle histology also showed marked amelioration of neurogenic muscle atrophy in the AR-97Q mice treated with 17-AAG (**Fig. 5d**). We confirmed a significant reduction of 1C2-positive nuclear accumulation in both spinal cord ($P < 0.01$) and skeletal muscle ($P < 0.05$) by quantitative assessment (**Fig. 5e**). AR-24Q mice and normal littermates treated with 17-AAG showed no altered phenotypes (data not shown).

To evaluate the toxic effects of 17-AAG, we examined blood samples from 25-week-old mice treated with 25 mg/kg 17-AAG for 20 weeks. Measurements of aspartate aminotransferase, alanine aminotransferase, blood urea nitrogen and serum creatinine showed that treatment with 17-AAG resulted in neither infertility nor liver or renal dysfunction in the AR-97Q male mice at the dose of 25 mg/kg (**Supplementary Fig. 2** online).

Mutant AR is preferentially degraded by 17-AAG *in vivo*

As the mutant AR was preferentially degraded as compared to the wild-type AR in the presence of 17-AAG *in vitro*, we also examined the level of AR in the SBMA mouse model. Western blot analysis of lysates of the spinal cord and muscle of AR-97Q mice showed high molecular–weight mutant AR protein complex retained in the stacking gel as well as a band of monomeric mutant AR, whereas only the band of wild-type monomeric AR was visible in tissues from the AR-24Q mice (**Fig. 6a,b**). Treatment with 17-AAG notably diminished both the high molecular–weight complex and the monomer of mutant AR in the spinal cord and muscle of the AR-97Q mice, but only slightly diminished the wild-type monomeric AR in AR-24Q mice (**Fig. 6a,b**). Treatment with 17-AAG decreased the amount of the monomeric AR in AR-97Q mice by 64.4% in the spinal cord and 45.0% in the skeletal muscle, whereas these amounts were only 25.9% and 12.5%, respectively, in AR-24Q mice (**Fig. 6a,b**). Thus, the reduction rate of the monomeric mutant AR was significantly higher than the wild-type

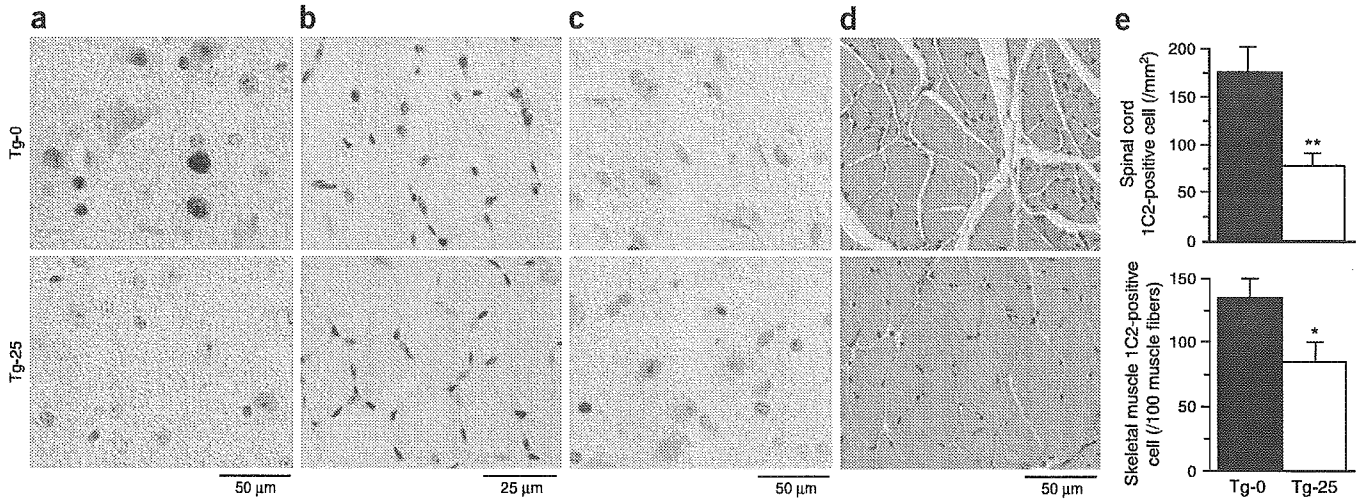

Figure 5 Effects of 17-AAG on the histopathology of male AR-97Q mice. **(a,b)** Immunohistochemical staining with 1C2-specific antibody showed marked differences in diffuse nuclear staining and nuclear inclusions between Tg-0 and Tg-25 mice in the spinal anterior horn and skeletal muscle, respectively. **(c)** Immunohistochemical staining with GFAP-specific antibody also showed an obvious reduction of reactive astrogliosis in the spinal anterior horn of mice treated with 17-AAG. **(d)** Hematoxylin and eosin staining of the muscle in Tg-0 mice showed obvious grouped atrophy and small angulated fibers, which were not seen in Tg-25 mice. **(e)** There was a significant reduction in 1C2-positive cell staining in the spinal cord ($P < 0.01$) and skeletal muscle ($P < 0.05$) in Tg-25 as compared to Tg-0 mice. Values are expressed as mean ± s.e.m. ($n = 6$). $^*P < 0.05$, $^{**}P < 0.01$.

AR in both spinal cord ($P < 0.001$) and skeletal muscle ($P < 0.01$; **Fig. 6c**). The levels of wild-type and mutant *AR* mRNA were similar in the respective mice treated with 17-AAG (**Fig. 6d**). We also performed filter-trap assays for quantitative analyses of both the large molecular aggregated and soluble forms of the mutant AR[36]. Both forms of trapped AR-97Q protein were markedly reduced in the spinal cord and muscle of Tg-25 mice, whereas those from the AR-24Q were not (**Supplementary Fig. 3** online). These observations strongly indicate that 17-AAG markedly reduces not only the monomeric mutant AR protein but also the high molecular–weight mutant AR complex, because of the preferential degradation of the mutant AR.

Western blot analysis showed that the levels of Hsp70 and Hsp40 in spinal cord were increased by 47.1% and 29.5%, respectively, and in muscle by 29.2% and 24.7%, respectively (**Supplementary Fig. 4** online) after treatment with 17-AAG. These pharmacological effects of chaperone induction were statistically significant ($P < 0.05$ for all parameters), but not as marked as the 17-AAG–induced mutant AR reduction, and were also not as pronounced as those arising from genetic manipulation in our previous study[36].

Hsp90 inhibitors nonspecifically activate heat shock responses through a dissociation of the heat-shock transcription factor (HSF-1) from the Hsp90 complex[27,41]. Although the expression of

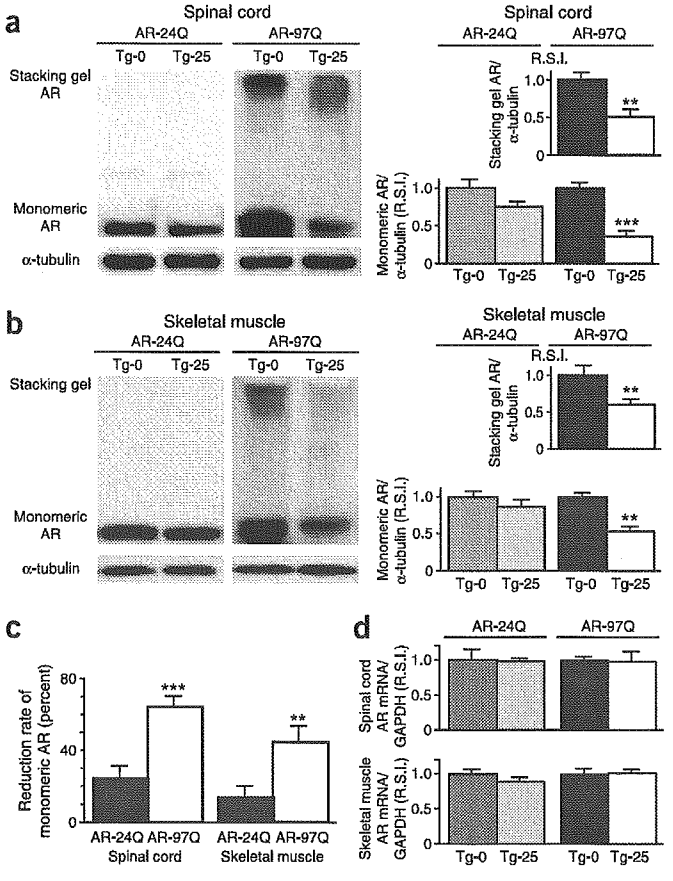

Figure 6 Effects of 17-AAG on AR expression in male AR-24Q or 97Q mice. **(a,b)** Western blot analysis of the spinal cord and muscle of AR-24Q and AR-97Q mice probed with AR-specific antibody. In both spinal cord and muscle of mice treated with 17-AAG, there was a significant decrease in the amount of mutant AR in the stacking gel and monomeric mutant AR in AR-97Q mice, but only slightly less monomeric wild-type AR in AR-24Q mice compared with that from untreated control mice. **(c)** Comparison of reduction rate of wild-type and mutant AR. Densitometric analysis showed that the 17-AAG–induced reduction of monomeric mutant AR was significantly greater than that of the wild-type monomeric AR. 17-AAG resulted in a 64.4% decline in monomeric mutant AR in the spinal cord, and a 45.0% decline in the skeletal muscle, whereas there was only a 25.9% decline in the spinal cord and a 12.5% decline in the skeletal muscle of AR-24Q mice. These results show significant differences of the reduction rate between wild-type and mutant AR in both spinal cord and skeletal muscle. Values are expressed as mean ± s.e.m. ($n = 5$). $^*P < 0.05$, $^{**}P < 0.01$, $^{***}P < 0.001$. **(d)** Real-time RT-PCR of wild-type and mutant *AR* mRNA *in vivo*. The expression levels of wild-type and mutant *AR* mRNA in transgenic mouse spinal cord and skeletal muscle were similar under 17-AAG treatments. Values are expressed as mean ± s.e.m. ($n = 3$).

Hsp90 and HSF-1 was not altered after 17-AAG treatment, coimmunoprecipitation of HSF-1 with Hsp90 in the spinal cord and skeletal muscle was significantly reduced ($P < 0.01$ for both) after 17-AAG treatment (**Supplementary Fig. 4** online), indicating that this drug induces Hsps through activation of HSF-1.

DISCUSSION

Our study showed that the polyQ-expanded mutant AR present in SBMA was preferentially degraded by treatment with 17-AAG. Elimination of mutant AR was mediated through its preferential incorporation into the Hsp90-chaperone complex, where it is then prone to proteasomal degradation. Owing to this mechanism, 17-AAG markedly ameliorated motor phenotypes of the SBMA mouse model without toxicity. Our present data from the mouse model also confirmed that 17-AAG passes through the blood-brain barrier as previously reported[42], and that it reaches a concentration high enough to have effects in the central nervous system.

Recently, some antitumor agents have been therapeutically applied to neurodegenerative diseases[43,44]. Most antitumor agents have some cytotoxic effects on normal cells, which must be overcome in any clinical application against neurodegeneration. Because neurodegenerative diseases generally follow a chronic progression and the medical treatment is, thus, long-standing compared to that for malignancy, the toxic side effects should be extensively suppressed. In contrast to general antitumor agents, the effects of 17-AAG have been known to have a high selectivity for tumor cells. This selectivity results from the high affinity of 17-AAG for the Hsp90 client oncoproteins when they are incorporated in the Hsp90-dependent multichaperone complex, thereby increasing their binding affinity for 17-AAG more than 100-fold[19]. This high selectivity of 17-AAG for the incorporated Hsp90 client protein eventually minimizes its toxic side effects and renders it very feasible for clinical applications, especially for neurodegenerative diseases. In fact, our transgenic mice were free from obvious side effects after the consecutive administration of 17-AAG for 20 weeks.

The major pharmacological effect of 17-AAG is to promote the dissociation of p23 from Hsp90 client protein complexes[10–12,16]. In this study, we showed that the mutant AR with an expanded polyQ had a higher association with p23 than did the wild-type AR. We consider this significantly higher association between the mutant AR and p23, particularly compared with the wild-type AR, to be the essential basis for preferential degradation of the polyQ-expanded mutant AR after 17-AAG treatment. Furthermore, the increase in Hop and decrease in p23 in the mutant AR-bound Hsp90 complex after 17-AAG treatment strongly supports the view that Hsp90 complexes were shifted to the proteasome-targeting form by 17-AAG, leading to proteasomal degradation of mutant AR. Given that the increase in Hop proteins in Hsp90 complexes and the decrease in p23 were only detected after the higher concentration of 17-AAG and after a very short period of incubation, this chaperone complex shift seems to be very rapid, as has been suggested previously[12].

Hsps, particularly Hsp70, have been shown to suppress aggregate formation and cellular toxicity in a wide range of polyQ disease models[21,36,45,46]. Geldanamycin has been considered a neuroprotective agent because of its ability to induce Hsp70 (refs. 22–24,27), and in polyQ diseases, has been proven to suppress aggregation of mutant huntingtin protein in a cultured-cell model through the induction of Hsp70 and Hsp40 (refs. 22,23). Hsp90 inhibitors have also been shown to be effective in animal models of Parkinson disease[24], stroke[27] and autoimmune encephalomyelitis[28]. It was thought that these effects were based only on the ability of the Hsp90 inhibitors to induce Hsps. As shown in this study, however, 17-AAG induced only limited amounts of Hsp70 and Hsp40 *in vivo*. Furthermore, our results suggest that the pathway for mutant AR degradation by 17-AAG through the Hsp90-client protein complex system is predominant. 17-AAG is expected to exert the most effective therapeutic potential for diseases in which the disease-causing protein belongs to the Hsp90 client protein family.

Mutant p53, which is present in nearly half of all malignancies and is an Hsp90 client protein, shows a much higher sensitivity to Hsp90 inhibitors than does wild-type p53 (ref. 47), just as AR, in its polyQ-expanded mutant form, acquired higher sensitivity to the Hsp90 inhibitor. In the case of neurodegenerative diseases, phosphorylated tau would be one of the target proteins of Hsp90 inhibitors, because geldanamycin substantially reduces the total amount of phosphorylated tau[25,26], and also inhibits tau aggregation[25]. According to these previous reports, our data suggest that 17-AAG would also be a candidate for a therapeutic approach to a wide range of tauopathies. The successful application of 17-AAG to polyQ diseases other than SBMA remains to be seen. But, as a previous report showed, the blockage of pathogenetic gene expression could reversibly reduce nuclear inclusions and reactive gliosis in a mouse model of Huntington disease by self-cleaning functions[48]. Indeed, one therapeutic approach, which directly reduced abnormal protein using RNA interference, proved to be beneficial in a mouse model of SCA1 (ref. 49). There is no doubt that the reduction of disease-causing protein would be beneficial in polyQ diseases. Therefore, once it is proven that the disease-causing proteins belong to the Hsp90 client protein family and have high affinities to Hsp90 inhibitors, 17-AAG is expected to preferentially degrade the expanded polyQ-containing disease proteins and, thus, would be a good candidate for clinical therapeutics.

In conclusion, we have shown the efficacy and safety of 17-AAG in a model mouse of SBMA, a neurodegenerative disease, and considerably extended the therapeutic application of 17-AAG beyond oncological diseases. In addition, we have documented the differential degradation efficacy of a polyQ-expanded mutant protein compared with its wild-type form. This strategy is apparently different from the previous strategy for polyQ diseases, which unavoidably allowed abnormal protein to remain and placed much value mainly on the inhibition of protein aggregation. 17-AAG, directly reducing disease-causing protein itself, presents a new therapeutic avenue for SBMA, and has potentially widespread application for other neurodegenerative diseases.

METHODS

DNA transfection. We constructed full-length ARs by subcloning AR inserts derived from pSP64-AR24 or pSP64-AR97 (ref. 46) into the pCR3.1 mammalian expression vector (Invitrogen). We plated SH-SY5Y cells in 6-cm dishes and transfected each dish with 8 μg of the vector containing AR24 or AR97 using Lipofectamine 2000 (Invitrogen) according to the manufacturer's instructions. We cultured the cells for 48 h. In this culture system, we detected a band of monomeric mutant AR in the separating gel, but could hardly detect the high molecular-weight mutant AR protein complex, which was retained in the stacking gel.

Neurological and behavioral assessment of SBMA model mice. We generated and maintained the AR-24Q and AR-97Q mice as previously described[35] (**Supplementary Methods** online). All animal experiments were performed in accordance with the National Institutes of Health Guide for the Care and Use of Laboratory Animals and under the approval of the Nagoya University Animal Experiment Committee. We performed the mouse rotarod task and cage activity as described previously[35]. The investigators in the behavioral assessment were blinded to the treatments.

Therapeutic agents and protocol for administration. We obtained 17-AAG, also known as NSC 330507, from the Regulatory Affairs Branch, Division of

Cancer Treatment and Diagnosis, National Cancer Institute and Kosan Biosciences. For cultured-cell models, we diluted a 1.8 mM stock solution of 17-AAG in DMSO into fresh medium to give final concentrations of 18–360 nM. In the cycloheximide study, we treated cells for 48 h with 17-AAG in the presence of 5 μg/ml cycloheximide (Sigma). To show pharmacological changes in the AR-Hsp90 complex, we exposed cultured cells for 30 min to 17-AAG at concentrations of 0.36, 3.6 and 36 μM 48 h after transfection. In the proteasome-inhibitory study, we exposed cultured cells for 6 h to 36 μM 17-AAG, and 5, 10 and 20 μM MG132 (Sigma) beginning 48 h after transfection.

For mouse models, we stored 50 mg/ml stock solutions of 17-AAG dissolved in DMSO at –20 °C. We began 17-AAG treatments when mice attained the age of 5 weeks, and continued them until mice were 25 weeks old. Normal male littermates, AR-24Q mice and AR-97Q mice received 50 μl intraperitoneal injections of 2.5 or 25 mg/kg 17-AAG three times a week on alternate days; control mice received DMSO alone.

Protein expression analysis. We lysed cells in CelLytic-M Mammalian Cell Lysis/Extraction Reagent (Sigma) and centrifuged them at 15,000*g* for 15 min at 4 °C. We homogenized the tissues from 16-week-old mice in CelLytic-M (Sigma) and centrifuged them at 2,500*g* for 15 min at 4 °C. Primary antibodies were as follows: AR-specific antibody (N-20 or H280; Santa Cruz); Hsp70-specific antibody (SPA-810; Stressgen); Hsp40-specific antibody (SPA-400; Stressgen); Hsp90-specific antibody (SPA-835; Stressgen); Hop-specific antibody (SRA-1500; Stressgen); p23-specific antibody (MA3-414; Affinity BioReagents); HSF-1–specific antibody (SPA-901; Stressgen); p85-specific antibody (Upstate); and α-tubulin–specific antibody (T9026; Sigma). We used the LAS-3000 imaging system to produce digital images and to quantify band intensities, which we then analyzed with Image Gauge software version 4.22 (Fujifilm). Densitometric values of AR, Hsp70, Hsp40 and Hsp90 were normalized to those of endogenous p85 or α-tubulin. Relative signal intensity (R.S.I.) was computed as the signal intensity of each sample divided by that of DMSO-treated cells or DMSO-treated mice.

We performed immunoprecipitation from cultured cells using 300 μg total protein lysate from cells, 10 μl Protein G Sepharose (Amersham) and 5 μl AR-specific antibody (N-20). For experiments involving coprecipitation of AR, we lysed cells in molybdate-containing lysis buffer[11,12,16]. Immunoprecipitation from mouse tissues was performed using 1 mg total protein lysed in CelLytic-M (Sigma). R.S.I. was computed as the signal intensity of each sample divided by that of AR-24Q cells, DMSO-treated cells or DMSO-treated mice.

Pulse-chase labeling assay. We transfected cells as described above, starved them for 1 h, and then labeled them for 1 h with 150 μCi of Redivue Pro-Mix L-[35S] *in vitro* cell-labeling mix (Amersham) per milliliter. We chased the cells for the indicated time intervals in complete medium with DMSO or 360 nM 17-AAG. We performed immunoprecipitation using equivalent amounts of protein lysates as described above, and analyzed by phosphorimaging (Typhoon 8600 phosphorimager; Amersham) and Image Gauge software, version 4.22 (Fujifilm).

Quantitative real-time RT-PCR. We determined the levels of AR mRNA by real-time Taqman PCR by the iCycler system (Bio-Rad) as previously described[50]. R.S.I. was computed as the signal intensity of each sample divided by that of DMSO-treated cells or DMSO-treated control mice.

Immunohistochemistry and histopathology. We prepared tissues as previously described[35–38]. We incubated the tissue sections with expanded polyQ-specific antibody (1:10,000, 1C2; Chemicon) and GFAP-specific antibody (1:1,000, Boehringer Manheim). We air-dried 6 μm–thick paraffin-embedded sections of the gastrocnemius muscles and stained them with hematoxylin and eosin. For quantification of 1C2-positive cells, we counted the number of 1C2-positive cells of the thoracic spinal cord and gastrocnemius muscle in each individual mouse as previously described[36].

Statistical analysis. We analyzed data by unpaired *t*-tests and Kaplan-Meier and log-rank tests for survival rate using Statview software version 5 (HULINKS). We examined statistical significance of the drug-dose dependency by the Williams test for multiple comparisons using Microsoft Excel 2004 (Microsoft).

Accession codes. BIND identifiers (http://bind.ca): 316918.

Note: Supplementary information is available on the Nature Medicine website.

ACKNOWLEDGMENTS

We thank National Cancer Institute and Kosan Biosciences for kindly providing 17-AAG. This work was supported by a Center of Excellence (COE) grant from the Ministry of Education, Culture, Sports, Science and Technology, Japan, and by grants from the Ministry of Health, Labor and Welfare, Japan.

COMPETING INTERESTS STATEMENT

The authors declare that they have no competing financial interests.

Published online at http://www.nature.com/naturemedicine/
Reprints and permissions information is available online at http://npg.nature.com/reprintsandpermissions/

1. Pratt, W.B. & Toft, D.O. Regulation of signaling protein function and trafficking by the hsp90/hsp70-based chaperone machinery. *Exp. Biol. Med. (Maywood)* **228**, 111–133 (2003).
2. Neckers, L., Schulte, T.W. & Mimnaugh, E. Geldanamycin as a potential anti-cancer agent: its molecular target and biochemical activity. *Invest. New Drugs* **17**, 361–373 (1999).
3. Supko, J.G., Hickman, R.L., Grever, M.R. & Malspeis, L. Preclinical pharmacologic evaluation of geldanamycin as an antitumor agent. *Cancer Chemother. Pharmacol.* **36**, 305–315 (1995).
4. Schulte, T.W. & Neckers, L.M. The benzoquinone ansamycin 17-allylamino-17-demethoxygeldanamycin binds to HSP90 and shares important biologic activities with geldanamycin. *Cancer Chemother. Pharmacol.* **42**, 273–279 (1998).
5. Page, J. *et al.* Comparison of geldanamycin (NSC-122750) and 17-allylaminogeldanamycin (NSC-330507D) toxicity in rats. *Proc. Am. Assoc. Cancer Res.* **38**, 308 (1997).
6. Sullivan, W. *et al.* Nucleotides and two functional states of hsp90. *J. Biol. Chem.* **272**, 8007–8012 (1997).
7. Bagatell, R. *et al.* Destabilization of steroid receptors by heat shock protein 90-binding drugs: a ligand-independent approach to hormonal therapy of breast cancer. *Clin. Cancer Res.* **7**, 2076–2084 (2001).
8. Neckers, L. Heat shock protein 90 inhibition by 17-allylamino-17-demethoxygeldanamycin: a novel therapeutic approach for treating hormone-refractory prostate cancer. *Clin. Cancer Res.* **8**, 962–966 (2002).
9. Felts, S.J. & Toft, D.O. p23, a simple protein with complex activities. *Cell Stress Chaperones* **8**, 108–113 (2003).
10. Johnson, J.L. & Toft, D.O. Binding of p23 and hsp90 during assembly with the progesterone receptor. *Mol. Endocrinol.* **9**, 670–678 (1995).
11. Smith, D.F. *et al.* Progesterone receptor structure and function altered by geldanamycin, an hsp90-binding agent. *Mol. Cell. Biol.* **15**, 6804–6812 (1995).
12. Whitesell, L. & Cook, P. Stable and specific binding of heat shock protein 90 by geldanamycin disrupts glucocorticoid receptor function in intact cells. *Mol. Endocrinol.* **10**, 705–712 (1996).
13. Schneider, C. *et al.* Pharmacologic shifting of a balance between protein refolding and degradation mediated by Hsp90. *Proc. Natl. Acad. Sci. USA* **93**, 14536–14541 (1996).
14. Solit, D.B. *et al.* 17-Allylamino-17-demethoxygeldanamycin induces the degradation of androgen receptor and HER-2/neu and inhibits the growth of prostate cancer xenografts. *Clin. Cancer Res.* **8**, 986–993 (2002).
15. Vanaja, D.K., Mitchell, S.H., Toft, D.O. & Young, C.Y. Effect of geldanamycin on androgen receptor function and stability. *Cell Stress Chaperones* **7**, 55–64 (2002).
16. Beliakoff, J. *et al.* Hormone-refractory breast cancer remains sensitive to the antitumor activity of heat shock protein 90 inhibitors. *Clin. Cancer Res.* **9**, 4961–4971 (2003).
17. Bonvini, P., Dalla Rosa, H., Vignes, N. & Rosolen, A. Ubiquitination and proteasomal degradation of nucleophosmin-anaplastic lymphoma kinase induced by 17-allylamino-demethoxygeldanamycin: role of the co-chaperone carboxyl heat shock protein 70-interacting protein. *Cancer Res.* **64**, 3256–3264 (2004).
18. Mimnaugh, E.G., Chavany, C. & Neckers, L. Polyubiquitination and proteasomal degradation of the p185c-erbB-2 receptor protein-tyrosine kinase induced by geldanamycin. *J. Biol. Chem.* **271**, 22796–22801 (1996).
19. Kamal, A. *et al.* A high-affinity conformation of Hsp90 confers tumour selectivity on Hsp90 inhibitors. *Nature* **425**, 407–410 (2003).
20. Whitesell, L., Bagatell, R. & Falsey, R. The stress response: implications for the clinical development of hsp90 inhibitors. *Curr. Cancer Drug Targets* **3**, 349–358 (2003).
21. Muchowski, P.J. & Wacker, J.L. Modulation of neurodegeneration by molecular chaperones. *Nat. Rev. Neurosci.* **6**, 11–22 (2005).
22. Sittler, A. *et al.* Geldanamycin activates a heat shock response and inhibits huntingtin aggregation in a cell culture model of Huntington's disease. *Hum. Mol. Genet.* **10**, 1307–1315 (2001).
23. Hay, D.G. *et al.* Progressive decrease in chaperone protein levels in a mouse model of Huntington's disease and induction of stress proteins as a therapeutic approach. *Hum. Mol. Genet.* **13**, 1389–1405 (2004).
24. Auluck, P.K. & Bonini, N.M. Pharmacological prevention of Parkinson disease in *Drosophila*. *Nat. Med.* **8**, 1185–1186 (2002).
25. Dou, F. *et al.* Chaperones increase association of tau protein with microtubules. *Proc. Natl. Acad. Sci. USA* **100**, 721–726 (2003).

26. Petrucelli, L. *et al.* CHIP and Hsp70 regulate tau ubiquitination, degradation and aggregation. *Hum. Mol. Genet.* **13**, 703–714 (2004).
27. Lu, A., Ran, R., Parmentier-Batteur, S., Nee, A. & Sharp, F.R. Geldanamycin induces heat shock proteins in brain and protects against focal cerebral ischemia. *J. Neurochem.* **81**, 355–364 (2002).
28. Murphy, P. *et al.* Suppressive effects of ansamycins on inducible nitric oxide synthase expression and the development of experimental autoimmune encephalomyelitis. *J. Neurosci. Res.* **67**, 461–470 (2002).
29. La Spada, A.R., Wilson, E.M., Lubahn, D.B., Harding, A.E. & Fischbeck, K.H. Androgen receptor gene mutations in X-linked spinal and bulbar muscular atrophy. *Nature* **352**, 77–79 (1991).
30. Sobue, G. *et al.* X-linked recessive bulbospinal neuronopathy. A clinicopathological study. *Brain* **112**, 209–232 (1989).
31. Zoghbi, H.Y. & Orr, H.T. Glutamine repeats and neurodegeneration. *Annu. Rev. Neurosci.* **23**, 217–247 (2000).
32. Tanaka, F. *et al.* Founder effect in spinal and bulbar muscular atrophy (SBMA). *Hum. Mol. Genet.* **5**, 1253–1257 (1996).
33. Doyu, M. *et al.* Severity of X-linked recessive bulbospinal neuronopathy correlates with size of the tandem CAG repeat in androgen receptor gene. *Ann. Neurol.* **32**, 707–710 (1992).
34. Adachi, H. *et al.* Widespread nuclear and cytoplasmic accumulation of mutant androgen receptor in SBMA patients. *Brain* **128**, 659–670 (2005).
35. Katsuno, M. *et al.* Testosterone reduction prevents phenotypic expression in a transgenic mouse model of spinal and bulbar muscular atrophy. *Neuron* **35**, 843–854 (2002).
36. Adachi, H. *et al.* Heat shock protein 70 chaperone overexpression ameliorates phenotypes of the spinal and bulbar muscular atrophy transgenic mouse model by reducing nuclear-localized mutant androgen receptor protein. *J. Neurosci.* **23**, 2203–2211 (2003).
37. Katsuno, M. *et al.* Leuprorelin rescues polyglutamine-dependent phenotypes in a transgenic mouse model of spinal and bulbar muscular atrophy. *Nat. Med.* **9**, 768–773 (2003).
38. Minamiyama, M. *et al.* Sodium butyrate ameliorates phenotypic expression in a transgenic mouse model of spinal and bulbar muscular atrophy. *Hum. Mol. Genet.* **13**, 1183–1192 (2004).
39. Bailey, C.K., Andriola, I.F., Kampinga, H.H. & Merry, D.E. Molecular chaperones enhance the degradation of expanded polyglutamine repeat androgen receptor in a cellular model of spinal and bulbar muscular atrophy. *Hum. Mol. Genet.* **11**, 515–523 (2002).
40. Lieberman, A.P., Harmison, G., Strand, A.D., Olson, J.M. & Fischbeck, K.H. Altered transcriptional regulation in cells expressing the expanded polyglutamine androgen receptor. *Hum. Mol. Genet.* **11**, 1967–1976 (2002).
41. Zou, J., Guo, Y., Guettouche, T., Smith, D.F. & Voellmy, R. Repression of heat shock transcription factor HSF1 activation by HSP90 (HSP90 complex) that forms a stress-sensitive complex with HSF1. *Cell* **94**, 471–480 (1998).
42. Egorin, M.J. *et al.* Plasma pharmacokinetics and tissue distribution of 17-(allylamino)-17-demethoxygeldanamycin (NSC 330507) in CD2F1 mice1. *Cancer Chemother. Pharmacol.* **47**, 291–302 (2001).
43. Ravikumar, B. *et al.* Inhibition of mTOR induces autophagy and reduces toxicity of polyglutamine expansions in fly and mouse models of Huntington disease. *Nat. Genet.* **36**, 585–595 (2004).
44. Ferrante, R.J. *et al.* Chemotherapy for the brain: the antitumor antibiotic mithramycin prolongs survival in a mouse model of Huntington's disease. *J. Neurosci.* **24**, 10335–10342 (2004).
45. Cummings, C.J. *et al.* Chaperone suppression of aggregation and altered subcellular proteasome localization imply protein misfolding in SCA1. *Nat. Genet.* **19**, 148–154 (1998).
46. Kobayashi, Y. *et al.* Chaperones Hsp70 and Hsp40 suppress aggregate formation and apoptosis in cultured neuronal cells expressing truncated androgen receptor protein with expanded polyglutamine tract. *J. Biol. Chem.* **275**, 8772–8778 (2000).
47. Blagosklonny, M.V., Toretsky, J., Bohen, S. & Neckers, L. Mutant conformation of p53 translated *in vitro* or *in vivo* requires functional HSP90. *Proc. Natl. Acad. Sci. USA* **93**, 8379–8383 (1996).
48. Yamamoto, A., Lucas, J.J. & Hen, R. Reversal of neuropathology and motor dysfunction in a conditional model of Huntington's disease. *Cell* **101**, 57–66 (2000).
49. Xia, H. *et al.* RNAi suppresses polyglutamine-induced neurodegeneration in a model of spinocerebellar ataxia. *Nat. Med.* **10**, 816–820 (2004).
50. Ishigaki, S. *et al.* X-Linked inhibitor of apoptosis protein is involved in mutant SOD1-mediated neuronal degeneration. *J. Neurochem.* **82**, 576–584 (2002).

doi:10.1093/brain/awh605 *Brain* (2005), 128, 2518–2534

The wide spectrum of clinical manifestations in Sjögren's syndrome-associated neuropathy

Keiko Mori,[1] Masahiro Iijima,[1] Haruki Koike,[1] Naoki Hattori,[1] Fumiaki Tanaka,[1] Hirohisa Watanabe,[1] Masahisa Katsuno,[1] Asako Fujita,[2] Ikuko Aiba,[2] Akihiko Ogata,[3] Toyokazu Saito,[4] Kunihiko Asakura,[5] Mari Yoshida,[6] Masaaki Hirayama[1] and Gen Sobue[1]

[1]Department of Neurology, Nagoya University Graduate School of Medicine, [2]Department of Neurology, Higashi Nagoya Hospital, Nagoya, [3]Department of Neurology, Hokkaido University School of Medicine, Sapporo, Japan, [4]Rehabilitation Center, Kitasato University School of Medicine, Kanagawa, Japan, [5]Department of Microbiology and Immunology, Kanazawa Medical Collage, Kanazawa, Japan and [6]Department of Neuropathology, Institute for Medical Science of Aging, Aichi Medical University, Japan

Correspondence to: Gen Sobue MD, Department of Neurology, Nagoya University Graduate School of Medicine, 65 Tsurumai-cho, Showa-ku, Nagoya 466-8550, Japan
E-mail: sobueg@med.nagoya-u.ac.jp

We assessed the clinicopathological features of 92 patients with primary Sjögren's syndrome-associated neuropathy (76 women, 16 men, 54.7 years, age at onset). The majority of patients (93%) were diagnosed with Sjögren's syndrome after neuropathic symptoms appeared. We classified these patients into seven forms of neuropathy: sensory ataxic neuropathy ($n = 36$), painful sensory neuropathy without sensory ataxia ($n = 18$), multiple mononeuropathy ($n = 11$), multiple cranial neuropathy ($n = 5$), trigeminal neuropathy ($n = 15$), autonomic neuropathy ($n = 3$) and radiculoneuropathy ($n = 4$), based on the predominant neuropathic symptoms. Acute or subacute onset was seen more frequently in multiple mononeuropathy and multiple cranial neuropathy, whereas chronic progression was predominant in other forms of neuropathy. Sensory symptoms without substantial motor involvement were seen predominantly in sensory ataxic, painful sensory, trigeminal and autonomic neuropathy, although the affected sensory modalities and distribution pattern varied. In contrast, motor weakness and muscle atrophy were observed in multiple mononeuropathy, multiple cranial neuropathy and radiculoneuropathy. Autonomic symptoms were often seen in all forms of neuropathy. Abnormal pupils and orthostatic hypotension were particularly frequent in sensory ataxic, painful, trigeminal and autonomic neuropathy. Unelicited somatosensory evoked potentials and spinal cord posterior column abnormalities in MRI were observed in sensory ataxic, painful and autonomic neuropathy. Sural nerve biopsy specimens ($n = 55$) revealed variable degrees of axon loss. Predominantly large fibre loss was observed in sensory ataxic neuropathy, whereas predominantly small fibre loss occurred in painful sensory neuropathy. Angiitis and perivascular cell invasion were seen most frequently in multiple mononeuropathy, followed by sensory ataxic neuropathy. The autopsy findings of one patient with sensory ataxic neuropathy showed severe large sensory neuron loss paralleling to dorsal root and posterior column involvement of the spinal cord, and severe sympathetic neuron loss. Degrees of neuron loss in the dorsal and sympathetic ganglion corresponded to segmental distribution of sensory and sweating impairment. Multifocal T-cell invasion was seen in the dorsal root and sympathetic ganglion, perineurial space and vessel walls in the nerve trunks. Differential therapeutic responses for corticosteroids and IVIg were seen among the neuropathic forms. These clinicopathological observations suggest that sensory ataxic, painful and perhaps trigeminal neuropathy are related to ganglioneuronopathic process, whereas multiple mononeuropathy and multiple cranial neuropathy would be more closely associated with vasculitic process.

Keywords: angiitis; autonomic nerve dysfunction; ganglionopathy; neuropathy; Sjögren's syndrome

Abbreviations: CMAP = compound muscle action potential; DL = distal motor latency; MIGB = meta-iodobenzylguanidine; MCV = motor nerve conduction velocity; NCS = nerve conduction studies; SNAP = sensory nerve action potential; SCV = sensory nerve conduction velocity; SEP = somatosensory evoked potential

Received April 19, 2005. Revised June 20, 2005. Accepted June 30, 2005. Advance Access publication July 27, 2005

Introduction

Primary Sjögren's syndrome is a systemic autoimmune disease characterized by xerophthalmia and xerostomia, and is associated with systemic visceral involvement, including pneumonitis, renal tubular acidosis, pancreatitis, myositis, and occasionally lymphocytic proliferation. A wide variety of neurological complications also are characteristic features of primary Sjögren's syndrome (Attwood *et al.*, 1961; Alexander *et al.*, 1982; Delalande *et al.*, 2004). Peripheral neuropathy is a major neurological manifestation of Sjögren's syndrome and its aetiology has been considered to be vasculitis in the peripheral nerves, similar to that observed in other collagen diseases. In 1986 and 1990, it was demonstrated that dorsal root ganglionitis with degeneration of dorsal root ganglion neurons and mononuclear cell infiltration without vasculitis are associated with the sensory ataxic form of Sjögren's syndrome-associated neuropathy, suggesting that ganglion neurons themselves can be a target of Sjögren's syndrome (Malinow *et al.*, 1986; Griffin *et al.*, 1990).

Sjögren's syndrome-associated neuropathy has been shown to manifest as a variety of forms of neuropathy, including sensory ataxic neuropathy (Kennett *et al.*, 1986; Griffin *et al.*, 1990; Kaplan *et al.*, 1990; Sobue *et al.*, 1993), trigeminal neuropathy (Kaltreider *et al.*, 1969), multiple mononeuropathy (Peyronnard *et al.*, 1982; Molina *et al.*, 1985), radiculoneuropathy (Gross *et al.*, 1987; Grant *et al.*, 1997), painful sensory neuropathy without sensory ataxia (Denislic *et al.*, 1995; Mori *et al.*, 2003), autonomic neuropathy with anhidrosis (Kumazawa *et al.*, 1993; Goto *et al.*, 2000) and multiple cranial neuropathy (Touze *et al.*, 1999; Chu *et al.*, 2000; Urban *et al.*, 2001). While the wide spectrum of these neuropathies has been described in anecdotal reports or in studies of the systemic manifestations of Sjögren's syndrome (Mellgren *et al.*, 1989; Gemignani *et al.*, 1994; Mauch *et al.*, 1994), the pathogenic mechanism responsible for most forms of Sjögren's syndrome-associated neuropathy remains unresolved. Furthermore, the spectrum of neuropathy and neuropathic symptoms of each form of neuropathy, particularly in the pathological and electrophysiological background, have not been well elucidated. In addition, since the prevalence of Sjögren's syndrome is growing in the elderly (Lafitte *et al.*, 2001), Sjögren's syndrome-associated neuropathy also has become more prevalent. It is therefore necessary to re-evaluate the clinical spectrum, and pathological and electrophysiological features of Sjögren's syndrome-associated neuropathy.

In this study, we assessed the clinicopathological and electrophysiological features of a large number of patients associated with primary Sjögren's syndrome-associated neuropathy and determined the range of clinical manifestations of neuropathy.

Patients and methods

Patients

A total of 92 patients (76 women, 16 men; mean age, 59.7 years), all of Japanese descent, who fulfilled the diagnostic criteria for primary Sjögren's syndrome and who had been referred to the Hospital of Nagoya University School of Medicine and its affiliated hospitals between 1985 and 2004 were the subjects of this study. The diagnosis of primary Sjögren's syndrome was established by the criteria proposed by the Diagnostic Committee of Health and Welfare of Japan (Fujibayashi *et al.*, 1999) and by the American-European Community (Vitali *et al.*, 2002). These criteria included symptoms of xerophthalmia and xerostomia, objective evidence of keratoconjunctivitis such as an abnormal Schirmer's test and an abnormal Rose Bengal score, evidence of chronic lymphocytic sialoadenitis on a minor salivary grand biopsy specimen, abnormal salivary gland scintigraphy or sialography, decreased salivary flow determined by a gum test and the presence of either anti-Sjögren's syndrome A or B (anti-SS-A or SS-B) autoantibodies (Fujibayashi *et al.*, 1999; Vitali *et al.*, 2002). Patients with other collagen diseases, such as systemic lupus erythematosus, rheumatoid arthritis, mixed connective tissue disease, progressive systemic sclerosis, polyarteritis nodosa, polymyositis and Churg–Strauss syndrome, diagnosed by the diagnostic criteria appropriate to each condition (Anonymous, 1980; Tan *et al.*, 1982; Arnett *et al.*, 1988; Masi *et al.*, 1990) and designated as having secondary Sjögren's syndrome, were excluded from this study. Patients underwent neurological examinations, blood studies, CSF studies, nerve conduction studies (NCS), sural nerve biopsies, somatosensory evoked potentials (SEPs) and spinal MRI.

A patient with the sensory ataxic form of Sjögren's syndrome-associated neuropathy who died at 88 years of age underwent autopsy and histological examination.

Assessment of neurological symptoms, activities of daily living and autonomic nerve dysfunction

Neurological examinations for somatic motor and sensory symptoms were performed by at least one neurologist. Sensory examinations were performed for light touch, pinprick, vibratory sensation and joint position sense, as well as for the presence of sensory ataxia and pain or painful dysaesthesia. Muscle strength was assessed using the Medical Research Council scale. Cranial nerve function, Romberg's sign, walking pattern, deep tendon reflexes and pathological reflexes were also assessed. Autonomic symptoms were assessed as described elsewhere.

For the assessment of clinical disability on daily life the modified Rankin scale (van Swieten *et al.*, 1988) was used. For the assessment of autonomic nerve dysfunction, we evaluated pupil abnormalities, including presence of Adie's pupils, anisocoria and elliptic pupils, urinary disturbances, diarrhoea and constipation, hypohidrosis and anhidrosis, orthostatic hypotension and ^{123}I-meta-iodobenzylguanidine (MIBG) cardiac accumulation. Autonomic symptoms generally were assessed by examining or interviewing patients or interviewing patients' family members, or reviewing the clinical records. Urinary symptoms were estimated by nocturnal or diurnal urinary frequency, a sensation of urgency, urinary incontinence, voiding difficulty and retention. Constipation was considered to be present if there were no stools for more than 3 days. Orthostatic hypotension was defined as a fall in systolic blood pressure of $\geq$30 mmHg upon standing from a recumbent position. For assessment of ^{123}I-MIBG cardiac accumulation, ^{123}I-MIBG 111 mBq (myo-MIBG-^{123}I for injection; Daiichi Radioisotope Laboratories Co.,

Tokyo, Japan) was given intravenously in Lugol's solution (200 mg iodine) to block the thyroid uptake. Cardiac MIBG uptake was expressed as a heart/ mediastinum ratio (H/M ratio) at 30 min (early scan) and 4 h (delayed scan) as described before (Watanabe *et al.*, 2001). Thermography and quantitative sweating measurements were performed on some selected patients as previously described (Kumazawa *et al.*, 1993).

Nerve conduction studies and somatosensory evoked potentials

Motor and sensory NCS were performed in the median, tibial and sural nerves using a standard method as described before (Sobue *et al.*, 1989). Motor nerve conduction velocity (MCV), distal motor latency (DL) and compound muscle action potential (CMAP) were recorded for the median and tibial nerves. Sensory nerve conduction velocity (SCV) and sensory nerve action potential (SNAP) were assessed for the median and sural nerves. Control values were obtained in 191 normal volunteers (mean age ± SD, 48.7 ± 16.5 years; men : women, 97 : 94) for the median nerve, 121 (mean age ± SD, 49.9 ± 15.0; men : women, 64 : 57) for the tibial nerve and 133 (mean age ± SD, 50.6 ± 15.6; men : women, 74 : 59) for the sural nerve (Koike *et al.*, 2001). Blink reflexes were recorded using a standard technique (Kimura, 2001).

SEPs were recorded using median nerve stimulation at the wrist (Kachi *et al.*, 1994). Cortical (N20), cervical (N13), and Erb's point (N9) peaks were assessed by separate stimulation. Controls of the latency of SEPs were obtained in 37 normal volunteers (mean age ± SD, 38 ± 7 years).

Sural nerve biopsy and autopsy study

Sural nerve biopsies were performed in 55 patients as described previously (Sobue *et al.*, 1989). Informed consent was established beforehand. Sural nerve biopsy specimens were examined by standard light microscopic methods and by teased fibre techniques. Specimens were divided into two portions. The first portion was fixed in 2.5% glutaraldehyde solution in 0.125 M cacodylate buffer (pH 7.4) and then embedded in an epoxy resin for morphometric and ultrastructural study. Density of myelinated fibres and morphological features were assessed in sections embedded in the epoxy resin and stained with toluidine blue using a computer-assisted image analyser (Luzex FS; Nikon, Tokyo, Japan), and densities of small and large myelinated fibres were calculated as described previously (Sobue *et al.*, 1989; Koike *et al.*, 2001). Some parts of specimens were processed for teased fibre study and were assessed for pathological conditions according to criteria described previously (Sobue *et al.*, 1989; Dyck *et al.*, 1993). For electron microscopic examination, epoxy resin-embedded specimens were processed for ultrathin sectioning. To assess the density of unmyelinated fibres, electron microscopic photomicrographs at a magnification of ×4000 were taken in random fashion to cover the ultrathin transverse section. The density of the unmyelinated fibres was estimated from the photomicrographs using a computer-assisted image analysis system.

For the autopsy study, the brain, spinal cord, sympathetic and sensory ganglia, peripheral nerve trunks, submandibular and subauricular salivary glands as well as various visceral organs were sampled systemically at the time of autopsy and examined in paraffin and epoxy-resin embedded sections.

MRI assessment of cervical spinal cord

A total of 27 patients underwent MRI of the cervical spinal cord, including the C4 level on a 1.5 T unit. We used axial T2*-weighted gradient echo images (repetition time/echo time/excitations, 700/21/3; flip angle, 20°; matrix, 256 × 256) as described previously (Yasuda *et al.*, 1994; Sobue *et al.*, 1995; Mori *et al.*, 2001). MRI findings were assessed on their distributions of abnormal high intensity area in the posterior columns of the spinal cord.

Laboratory data

Routine blood tests were performed, including anti-SS-A and anti-SS-B antibodies. These autoantibodies were detected using enzyme-linked immunosorbent assay and immunoblotting [Mesacup-2 test, according to the manufacturer's instructions (MBL, Ltd. Japan)]. Alpha-fodrin, a candidate autoantigen for Sjögren's syndrome (Haneji *et al.*, 1997) also was examined as follows. The purified recombinant N-terminal portion of alpha-fodrin and GST (glutathione-*S*-transferase) fusion protein (JS-1) were loaded onto 10% polyacrylamide gels and transferred to nitrocellulose membranes by electroblotting. The membranes were blocked overnight at room temperature with Tris-buffered saline containing 3% non-fat dry milk. The membranes were incubated with sera from patients with Sjögren's syndrome (1 : 200 dilution) for 4 h at room temperature. Then, bound antibodies were detected with biotinylated anti-human IgG antibodies and alkaline phosphatase-conjugated streptavidin (both from Jackson Immunoresearch, West Grove, PA) using 5-bromo-4-chloro-3-indolyl phosphate and nitro blue tetrazorium as substrates.

Statistical analysis

All statistical analyses were performed using the Mann–Whitney *U*-test. *P*-values of <0.05 were considered significant.

Results

General clinical features and classification of neuropathy

All 92 patients fulfilled the diagnostic criteria for Sjögren's syndrome (Fujibayashi *et al.*, 1999; Vitali *et al.*, 2002). The majority of patients (86 patients) were diagnosed as having Sjögren's syndrome after neurological symptoms developed, while only six patients were diagnosed with Sjögren's syndrome before the neurological symptoms appeared. Thus most of the patients had been followed for a neuropathy of unknown cause for a while before being diagnosed with Sjögren's syndrome. We classified these patients into seven forms of neuropathy: sensory ataxic neuropathy, painful sensory neuropathy without sensory ataxia, multiple mononeuropathy, multiple cranial neuropathy, trigeminal neuropathy, autonomic neuropathy and radiculoneuropathy, based on the predominant neuropathic symptoms. Sensory ataxic neuropathy was defined as one with sensory neuropathy predominantly manifesting as impairment of joint-position sense leading to sensory ataxia but preserved muscle power, muscle volume and motor nerve function (Sobue *et al.*, 1993). A total of 36 patients were included in the sensory ataxic neuropathy group. Painful neuropathy without sensory ataxia (Mori

et al., 2003) was another form of sensory neuropathy but with predominant involvement of superficial sensation of pain and light touch sense without or with minor impairment of deep sensation resulting in a painful sensory neuropathy without sensory ataxia. Motor function was well preserved with this neuropathy. Eighteen patients were included in this group. Eleven patients were considered to have multiple mononeuropathy. This form of neuropathy was characterized by multiple mononeuropathy mainly distributed in the distal portion of the limbs with both motor and sensory involvement. Sensory involvement generally included both superficial and deep sensation. Twenty patients were classified as having cranial neuropathy. Of the 20, 5 patients had multiple cranial neuropathy and 15 patients had isolated trigeminal neuropathy. Multiple cranial neuropathy affects multiple cranial motor and sensory nerves including the trigeminal nerve. Trigeminal neuropathy was defined as a pure sensory neuropathy restricted to the territory of the sensory trigeminal nerves. Autonomic neuropathy was characterized by predominant autonomic dysfunction. Three patients were considered to have this neuropathy. Radiculoneuropathy was defined by lesions restricted predominantly to the spinal roots or the very proximal portion of the spinal nerves. Radiculoneuropathy often mimics chronic inflammatory demyelinating polyneuropathy. Four patients were included in this category of neuropathy.

The age at first examination and the age of onset of neuropathic symptoms varied to some extent, but did not differ among the forms of neuropathy (Table 1). A female predominance was commonly observed in all of the neuropathies. Sjögren's syndrome-related symptoms also were seen at similar rates among the neuropathies. More than half of the patients had sicca syndrome, manifested by either xerophthalmia or xerostomia. Schirmer's test and the Rose Bengal test were positive in >50% of the examined patients. Almost all of the examined patients had either lymphocytic infiltration of the salivary glands, salivary gland cell destruction or both on minor salivary gland biopsy. Sialography and salivary scintigraphy also were positive in a majority of patients in each neuropathic group. Antibodies to SS-A and SS-B were present in 20–100% and 0–50% of patients in each neuropathic group, respectively. Only 13 patients were both SS-A and SS-B positive. Anti-alpha-fodrin antibodies were detected in 60–100% of patients in each neuropathic group. This positive rate was extremely high as compared with those in the control group without neuropathy (<14% positive), while it was not significantly different between neuropathic groups. Mild increases in the CSF protein concentration were seen in some of the patients examined.

As complicating systemic inflammatory symptoms, hypothyroidism was seen in nine patients, dyshaematopoietic anaemia in two patients, interstitial pneumonia in three patients, myositis in one patient, liver dysfunction in four patients, pancreatitis in two patients, renal involvement in one patient and lymphoma in one patient (Table 1).

Neuropathic features of each form of neuropathy

Sensory ataxic neuropathy

A total of 36 patients had this form of neuropathy (Table 2). This neuropathy was characterized by sensory ataxia due to kinaesthetic deep sensory impairment without substantial motor symptoms. The initial symptom was usually paraesthesias in the digits of the foot or hand. These paraesthesias were often unilateral, and gradually spread to the limbs, trunk and face. In three patients, the initial paraesthesia was localized to the trigeminal nerve area. The time from the onset to the development of full-blown symptoms of sensory involvement was variable among the patients, weeks to months in four patients, but usually months to years. The sensory symptoms were mostly asymmetrical, segmental or multi-focal rather than presenting as a symmetrical polyneuropathy, particularly in the progression stage. Ten patients had trigeminal nerve involvement. Muscle weakness and mild atrophy were observed in four patients. Sensory impairment was mostly deep sensory predominant with Romberg's sign and pseudoathetosis being present in all of the patients. Pain or painful dysaesthesia was present in 18 patients. A total of 10 and 20 patients showed facial and truncal sensory involvement, respectively. There was generalized areflexia in all patients. The walking pattern was characteristic of sensory ataxia. In the patients with advanced disease, they were unable to walk and were wheel-chair bound.

With respect to autonomic symptoms, 17 of the 30 assessed patients exhibited abnormal pupils including Adie's pupils associated with anisocoric and elliptic pupils (Table 3). Orthostatic hypotension was present in 12 patients, mostly without syncope. Hypohidrosis or anhidrosis was observed in 21 patients, often with segmental anhidrosis in the trunk (Fig. 1). Marked decreases in ^{123}I-MIBG cardiac uptake were present in 8 of the 11 patients who were examined.

With respect to nerve conduction, SNAPs in the median and sural nerves were not evoked in 61 and 50% of patients, respectively (Table 4). In contrast, CMAPs were fairly well preserved in most patients. MCV and SCV were not slowed. Temporal dispersion of the CMAPs or conduction block was not seen. SEPs were not evoked in 67, 73 and 40% of the examined patients in N20, N13 and N9, respectively (Table 4). These conduction studies indicate that axonal features were almost exclusively present in this neuropathy, and the central rami of sensory ganglion neurons were also involved in parallel.

T2*-weighted MRI demonstrated posterior column high intensity signal in 9 of the 12 examined patients (Table 4; Fig. 1). The extent of dorsal column high intensity T2* signal was well correlated with the distribution and intensity of sensory involvement and sensory ataxia, indicating the presence of central rami involvement due to sensory ganglion neuron damage (Mori *et al.*, 2001).

Sural nerve biopsy was performed in 31 patients (Table 5). Total myelinated fibre density was variably reduced, ranging

Table 1 Clinical features of patients with peripheral neuropathy associated with Sjögren's syndrome

Clinical features	Sensory neuropathy		Multiple mononeuropathy (n = 11)	Cranial neuropathy		Autonomic neuropathy (n = 3)	Radiculo-neuropathy (n = 4)
	Ataxic (n = 36)	Painful (n = 18)		Multiple (n = 5)	Trigeminal (n = 15)		
Age (years)	65.2 ± 7.8	58.1 ± 15.9	59.1 ± 18.2	55.6 ± 12.7	55.6 ± 9.4	46.3 ± 18.0	57.0 ± 11.0
Age of onset of neuropathy (years)	64.9 ± 12.9	56.0 ± 13.8	58.1 ± 13.5	55.1 ± 14.8	51.7 ± 11.6	42.5 ± 17.4	49.0 ± 12.2
Sex, women:men (n)	26:10	16:2	10:1	4:1	15:0	2:1	3:1
Follow-up (years)	5.7 ± 4.6	3.6 ± 2.8	2.3 ± 1.3	5.2 ± 6.6	7.0 ± 4.1	1.7 ± 1.6	7.3 ± 3.8
(range) (years)	(1–18)	(1–12)	(1–4)	(1–7)	(2–10)	(1–3)	(3–10)
Sjögren's syndrome							
Dry eye: n (%)/dry mouth: n (%)	20 (56)/23 (64)	13 (72)/12 (67)	7 (64)/7 (64)	3 (60)/2 (40)	10 (67)/10 (67)	2 (67)/2 (67)	2 (50)/2 (50)
Positive findings							
Schirmer's test: n (%)	27/29 (93)	14/15 (93)	7/8 (88)	5/5 (100)	8/10 (80)	3/3 (100)	2/4 (50)
Rose Bengal test: n (%)	20/29 (69)	11/12 (92)	6/6 (100)	3/5 (60)	8/9 (89)	2/2 (100)	ND
Salivary gland biopsy: n (%)	26/28 (93)	13/16 (81)	8/9 (89)	5/5 (100)	11/11 (100)	2/2 (100)	4/4 (100)
Sialography, cintigraphy: n (%)	9/10 (90)	6/6 (100)	3/3 (100)	2/3 (67)	8/8 (100)	1/1 (100)	ND
SS-A: n (%)	19/36 (53)	7/18 (39)	7/11 (64)	1/5 (20)	6/15 (40)	2/3 (67)	4/4 (100)
SS-B: n (%)	4/36 (11)	3/18 (17)	2/11 (18)	1/5 (20)	0/15 (0)	1/3 (33)	2/4 (50)
Alpha-fodrin: n (%)	14/16 (88)	6/7 (86)	3/5 (60)	5/5 (100)	2/2 (100)	1/1 (100)	3/3 (100)
CSF protein elevation: n (%)	8/23 (35)	3/10 (30)	5/8 (63)	1/3 (33)	0/1 (0)	0/1 (0)	4/4 (100)
Associated symptoms (n)	T (4), P (2), Pa (2), L (3), Ly (1)	T (2), A (2), R (1), P (1), M (1)	T (2)	–	–	–	T (1), L (1)

n/n, positive patient number to all examined patient number. As for associated symptoms, T, hypothyroidism; P, interstitial pneumonia; Pa, pancreatitis; A, anaemia; M, myositis; L, liver dysfunction; Ly, lymphoma; R, renal involvement.

Table 2 Neuropathic symptoms

Clinical features	Sensory neuropathy		Multiple mononeuropathy	Cranial neuropathy		Autonomic neuropathy	Radiculo-neuropathy
	Ataxic (n = 36)	Painful (n = 18)	(n = 11)	Multiple (n = 5)	Trigeminal (n = 15)	(n = 3)	(n = 4)
Initial symptom							
Sensory disturbance: n (%)	36 (100)	3 (17)	11 (100)	0 (0)	15 (100)	0 (0)	4 (100)
Pain/painful dysaesthesia: n (%)	0 (0)	18 (100)	1 (9)	1 (20)	2 (13)	0 (0)	0 (0)
Weakness: n (%)	0 (0)	0 (0)	8 (73)	0 (0)	0 (0)	0 (0)	2 (50)
Autonomic symptoms: n (%)	0 (0)	1 (6)	0 (0)	0 (0)	0 (0)	3 (100)	0 (0)
Cranial nerve symptoms: n (%)	3* (8)	0 (0)	1 (9)*	5 (100)	15 (100)	0 (0)	1 (25)**
Initial progression							
Acute: n (%)	0 (0)	3 (17)	2 (18)	3 (60)	0 (0)	1 (33)	0 (0)
Subacute: n (%)	4 (11)	1 (6)	4 (36)	0 (0)	3 (20)	0 (0)	1 (25)
Chronic: n (%)	32 (89)	14 (78)	5 (45)	2 (40)	12 (80)	2 (67)	3 (75)
Cranial nerve involvement: n (nerve)	10 (V)	8 (V)	2 (V)	2 (III), 3 (V), 2 (VI), 3 (VII), 3 (IX), 3 (X), 1(XII)	15 (V)	1 (V)	1 (III)
Muscle weakness/atrophy: n (%)	4 (11)	1 (6)	10 (91)	0 (0)	0 (0)	0 (0)	2 (50)
Sensory impairment: n (%)	36 (100)	18 (100)	11 (100)	3 (60)	15 (100)	2 (67)	4 (100)
Modality							
Deep > superficial sensation: n (%)	33 (92)	0 (0)	1 (9)	0 (0)	0 (0)	1 (33)	3 (75)
Deep = superficial sensation: n (%)	3 (8)	0 (0)	7 (64)	0 (0)	0 (0)	1 (33)	1 (25)
Superficial > deep sensation: n (%)	0 (0)	18 (100)	3 (27)	3 (60)	15 (100)	0 (0)	0 (0)
Pain/painful dysaesthesia: n (%)	18 (50)	18 (100)	7 (64)	1 (20)	2 (13)	0 (0)	0 (0)
Sensory ataxia: n (%)	36 (100)	2 (11)	1 (9)	0 (0)	0 (0)	2 (67)	2 (50)
Distribution							
Face: n (%)	10 (28)	8 (44)	2 (18)	3 (60)	15 (100)	1 (33)	0 (0)
Trunk: n (%)	20 (56)	10 (56)	2 (18)	2 (40)	0 (0)	2 (67)	1 (25)
Limbs: n (%)	36 (100)	18 (100)	11 (100)	2 (40)	2 (13)	2 (67)	4 (100)
Areflexia: n (%)	36 (100)	9 (50)	7 (64)	0 (0)	0 (0)	2 (67)	4 (100)
Modified Rankin scale (mean ± SD)	3.3 ± 0.8	2.3 ± 0.8	2.3 ± 0.8	–	–	3.3 ± 1.2	2.3 ± 1.3
(range)	(2–5)	(1–4)	(1–3)			(2–4)	(1–4)

Cranial nerve symptoms in initial symptom: *, trigeminal nerve lesion; **, diplopia and ptosis. Modified Rankin scale: 0, asymptomatic; 1, non-disabling symptoms not interfering with lifestyle; 2, mildly disabling symptoms leading to some restrictions of lifestyle but not interfering with capacity to look after oneself; 3, moderately disabling symptoms significantly interfering with lifestyle or precluding totally independent existence; 4, moderately severe disability precluding independent existence while not requiring constant attention around the clock; 5, severe disability with total dependency requiring constant attention day and night.

Table 3 Autonomic symptoms

Clinical features	Sensory neuropathy		Multiple mononeuropathy	Cranial neuropathy		Autonomic neuropathy	Radiculo-neuropathy
	Ataxic (n = 30)	Painful (n = 16)	(n = 6)	Multiple (n = 5)	Trigeminal (n = 9)	(n = 3)	(n = 4)
Abnormal pupils: n	17	3	0	1	3	3	0
Orthostatic hypotension: n	12	5	0	0	3	3	0
Faint: n	0	0	0	0	0	3	0
Hypohidrosis/anhidrosis: n	21	10	3	2	4	3	2
Diarrhoea: n	6	0	1	0	1	3	0
Constipation: n	6	5	2	1	1	3	2
Vomiting: n	2	0	0	0	0	1	0
Urinary disturbance: n	1	3	0	0	0	2	1
Decreased uptake of ^{123}I-MIBG: n	8/11	5/7	ND	ND	ND	2/2	0/2
Total: n	21/30	11/16	3/6	2/5	4/9	3/3	2/4

Decreased uptake of ^{123}I-MIBG = the ^{123}I-MIBG heart/mediastinum ratio (H/M ratio) of delayed scan was <1.8 (control–2 SD) (Hamada et *al.*, 2003). n/n, positive patient number to all examined patient number; ND, not determined.

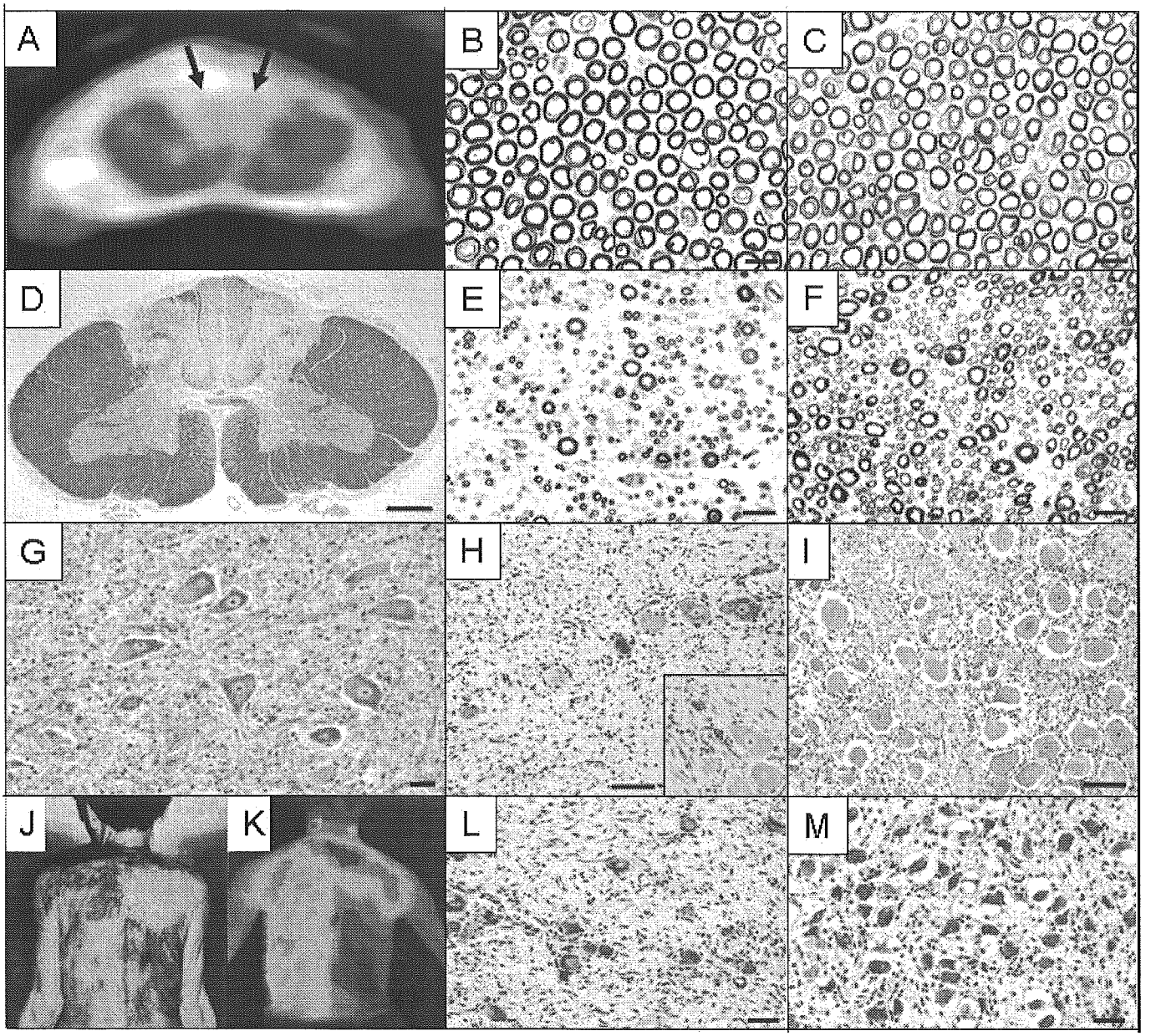

Fig. 1 Pathological findings, MRI and sweating assessment of an autopsied patient with the sensory ataxic neuropathy. (**A**) Axial T2*-weighted gradient echo image of the cervical spinal cord (C4) of the patient. A high intensity area is present in the posterior column including both fasciculus cuneatus and gracilis as indicated by arrows. (**B** and **C**) Cross-section of the L4 ventral spinal root. Myelinated fibres are well preserved in the patient (**B**) and control (**C**). Scale bar = 20 μm. (**D**) Cross-section of the dorsal column of the cervical spinal cord. Axons are almost completely lost. Klüver–Barrera's stain. Scale bar = 1 mm. (**E** and **F**) Cross-section of the L4 dorsal spinal root. Large myelinated fibres are severely lost in the patient (**E**) compared with the control (**F**). Scale bar = 20 μm. (**G**) Cross-section of the L4 ventral horn. The population of the anterior horn cell is well preserved. Klüver–Barrera's stain. Scale bar = 40 μm. (**H**) Cross-section of the L4 dorsal root ganglion. The population of the nerve cell is decreased (**H**). Nageotte's nodules are occasionally seen (**H**). (**I**) Control. Klüver–Barrera's stain. Scale bar = 100 μm. (**J**) Thermal sweating measured by Minor's iodine–starch test in an artificial climate chamber at an ambient temperature of 40°C and 40% relative humidity. The area of anhidrosis was very distinct and distributed in a segmental manner. (**K**) Plain thermograms monitored by infrared thermography. Surface skin temperature was also segmental in distribution (quoted from Kumazawa *et al.*, 1993 with permission for publication). (**L**) Section of the thoracic sympathetic ganglion. The population of the nerve cell bodies is decreased (**L**) compared with control case (**M**). Klüver–Barrera's stain. Scale bar = 40 μm.

from 131 to 6918/mm^2 (mean ± SD, 3287 ± 2843/mm^2), and that of unmyelinated fibres was also reduced. Mean densities of large, small myelinated and unmyelinated fibres were reduced to 18, 56 and 75% of normal controls, respectively, indicating large fibre predominant loss. Axonal sprouts were not conspicuous in any case. In teased-fibre preparations, axonal degeneration was observed in 30.9 ± 36.1% of samples, while segmental demyelination was seen in only

Table 4 Nerve conduction, sensory evoked potentials, and spinal cord MRI study

Nerve conduction, SEP and MRI	Sensory neuropathy		Multiple mononeuropathy	Cranial neuropathy		Autonomic neuropathy	Radiculo-neuropathy	Controls
	Ataxic	Painful		Multiple	Trigeminal			
Nerve conduction study	$n = 36$	$n = 18$	$n = 11$	$n = 5$	$n = 15$	$n = 3$	$n = 4$	$n = 121–191$
Median nerve								
MCV (m/s)	53.1 ± 4.0	53.3 ± 33.2	51.3 ± 3.7	51.2 ± 8.1	54.7 ± 3.5	53.2 ± 0.7	50.5 ± 10.3	57.8 ± 3.7
DL (ms)	3.7 ± 0.5	3.4 ± 0.2	3.5 ± 0.4	4.0 ± 0.5	3.9 ± 1.3	3.7 ± 0.6	4.4 ± 2.0	3.4 ± 0.4
CMAP (mV)	11.1 ± 2.8	11.2 ± 4.0	10.4 ± 2.4	11.4 ± 3.0	12.7 ± 3.4	10.5 ± 2.7	5.6 ± 3.1**	10.7 ± 3.5
SCV (m/s)	50.0 ± 4.7	51.5 ± 3.5	49.6 ± 7.8	61.4 ± 1.3	55.1 ± 2.6	58.5 ± 0.3	50.8 ± 9.5	57.8 ± 4.7
SNAP (μV)	4.1 ± 9.0***	4.4 ± 6.6***	4.9 ± 4.7***	23.9 ± 1.9	11.3 ± 4.1	25.6 ± 4.0	22.2 ± 1.0	23.5 ± 8.4
N.E. (%)	61	11	18	0	0	33	0	0
Tibial nerve								
MCV (m/s)	43.5 ± 2.8	44.5 ± 3.3	38.6 ± 3.9	48.3 ± 4.2	43.7 ± 2.3	44.7 ± 1.2	43.5 ± 1.1	46.9 ± 3.5
DL (ms)	4.8 ± 0.8	4.5 ± 0.4	5.1 ± 1.1	4.7 ± 1.0	5.1 ± 0.2	4.2 ± 0.9	6.0 ± 3.4	4.5 ± 0.8
CMAP (mV)	10.5 ± 7.0	14.5 ± 6.8	6.5 ± 9.1*	12.2 ± 9.1	16.4 ± 5.2	12.6 ± 1.0	9.2 ± 3.3*	10.9 ± 3.8
Sural nerve								
SCV (m/s)	45.3 ± 2.8	46.7 ± 6.5	46.4 ± 3.1	50.3 ± 3.5	53.4 ± 1.2	46.8 ± 0.0	45.0 ± 5.1	51.0 ± 5.1
SNAP (μV)	2.2 ± 3.6***	8.1 ± 8.1***	1.3 ± 1.5***	20.5 ± 3.5	22.5 ± 2.3	10.3 ± 1.4	18.3 ± 1.5	11.5 ± 4.7
N.E. (%)	50	17	55	0	0	33	0	0
SEP	$n = 15$	$n = 8$				$n = 3$	$n = 4$	$n = 37$
Median nerve stimulation								
N20 latency (ms)	20.2 ± 2.1	20.9 ± 2.3	ND	ND	ND	19.5 ± 0.7	21.4 ± 3.2	18.9 ± 1.1
N.E. (%)	67	0				33	0	
N13 latency (ms)	13.1 ± 0.8	14.4 ± 1.9	ND	ND	ND	13.1 ± 0.6	14.8 ± 2.6	12.8 ± 1.0
N.E. (%)	73	0				33	0	
N9 latency (ms)	9.1 ± 0.9	9.8 ± 0.9	ND	ND	ND	8.9 ± 0.4	10.1 ± 1.2	8.6 ± 0.6
N.E. (%)	40	13				33	0	
MRI	$n = 12$	$n = 8$				$n = 3$	$n = 4$	
Spinal cord abnormality	9†	3†	ND	ND	ND	1†	4‡	

Values are expressed as mean ± SD. Control values are those described previously (Koike *et al.*, 2001). MCV, motor nerve conduction velocity; DL, distal latency; CMAP, compound muscle action potentials; SCV, sensory nerve conduction velocity; SNAP, sensory nerve action potentials; N.E., not evoked; SEP, somatosensory evoked potentials; control values are from 37 conduction times. *$P < 0.05$, **$P < 0.01$, ***$P < 0.001$ as compared with control value. †In T2* weighted gradient echo images, a high intensity area is present in the posterior column. ‡In T1 weighted echo images. Posterior spinal roots and cauda equina are enhanced by gadolinium.

Table 5 Pathological findings in the sural nerve

Clinical features	Sensory neuropathy		Multiple mononeuropathy ($n = 8$)	Cranial neuropathy		Autonomic neuropathy ($n = 2$)	Radiculo-neuropathy ($n = 4$)	Controls ($n = 7$)
	Ataxic ($n = 31$)	Painful ($n = 9$)		Multiple ($n = 0$)	Trigeminal ($n = 1$)			
Myelinated fibre density (no./mm^2)								
Total	3287 ± 2843**	4105 ± 2260**	1153 ± 920**	ND	8010	2924	5985 ± 1890*	8220 ± 614
Large	579 ± 697***	2039 ± 1136*	226 ± 262**	ND	2994	1113	1593 ± 913*	3150 ± 383
Small	2878 ± 2482*	2056 ± 1267**	927 ± 672***	ND	5111	1811	4391 ± 977	5071 ± 397
Small/large	13.7 ± 18.1**	0.9 ± 0.5*	10.3 ± 12.0*	ND	1.7	2.9	3.1 ± 1.2	1.6 ± 0.2
Unmyelinated fibre density (no./mm^2)	22 643 ± 9477*	9879 ± 9203**	ND	ND		14 822	ND	29 901 ± 2623
Segmental de-/remyelination (%)	9.7 ± 9.4	10.0 ± 2.5	13.3 ± 13.1	ND	2.5	7.0	14.5 ± 9.2	7.2 ± 6.5
Axonal degeneration (%)	30.9 ± 36.1**	19.0 ± 16.1	61.0 ± 5.3**	ND	0	12.5	3.5 ± 4.9	1.4 ± 1.6
Vasculitis: n (%)	6 (19)	0 (0)	5 (63)	ND	0 (0)	0 (0)	0 (0)	–
Perivascular cell invasion: n (%)	9 (29)	1 (11)	6 (75)	ND	0 (0)	0 (0)	1 (25)	–

Values are expressed as mean ± SD. Control values (mean ± SD) were obtained from autopsy material and expressed as mean ± SD for 7 case. (Koike *et al.*, 2004). ND, not determined; Small < 6.73 μm; large ≥ 6.73 μm in fibre diameter (Sobue *et al.*, 1989); *$P < 0.05$, **$P < 0.01$, ***$P < 0.001$ as compared with control values.

9.7 ± 9.4% of samples, indicating that axonal changes are the predominant pathological feature. Chronic vasculitis of the arterioles in the epineurial space was seen in six patients and mild perivascular lymphocyte infiltrates in the small vessels were also seen in nine patients.

Painful sensory neuropathy without sensory ataxia

A total of 18 patients had this form of neuropathy (Table 2). The initial symptoms were painful dysaesthesia in the most distal portions of the limbs, usually in unilateral limbs. In three patients, the initial progression was acute, occurring in days, and painful dysaesthesias were present over the entire body, including the trunk and face. In a majority of patients, spread of the dysaesthesias was chronic, occurring over months to years. The trigeminal nerve was involved in eight patients. Sensory impairment was relatively predominant with respect to superficial sensation of pain, temperature and light touch, and was associated with pain or painful dysaesthesia. Deep sensation was relatively well preserved, and motor function also was preserved. However, mild sensory ataxia in the limbs was seen in two patients. The face and trunk were involved in 8 and 10 patients, respectively, and segmental in distribution in some patients. In contrast to the sensory ataxic form, deep tendon reflexes were fairly well preserved in half of the patients. Seven patients could not walk because of severe pain.

Eleven patients showed symptoms consistent with autonomic neuropathy (Table 3). Abnormal pupils, including Adie's pupils and elliptic pupils, were seen in three patients. Orthostatic hypotension and hypohidrosis or anhidrosis were present in 5 and 10 patients. Segmental distribution of anhidrosis was often seen in the trunk. A severe decrease in ^{123}I-MIBG cardiac uptake was seen in five of the seven examined patients. These results suggest that autonomic nerves are also widely involved in this form of neuropathy.

In contrast to sensory ataxic neuropathy, unelicited SNAPs were present in only 11 and 17% of median and sural nerves, respectively (Table 4). SCV was well preserved. MCV showed no slowing and CMAPs were well preserved. Cortical (N20) and cervical (N13) SEPs were elicited in all of the examined patients and Erb's point (N9) SEP was not elicited in only one patient examined.

T2*-MRI of the spinal cord showed minimal high intensity signal in the posterior column in three out of the eight patients studied (Table 4). The extent of high intensity signal in these patients was relatively small compared with those seen with sensory ataxic neuropathy. The sural nerve biopsy specimen in nine patients mostly showed small fibre loss (Table 5). Mean densities of large, small myelinated and unmyelinated fibres were reduced to 65, 41 and 33% of normal control, respectively, indicating small fibre predominant loss. Axonal sprouts were essentially absent. In teased-fibre preparations, axonal degeneration was seen in 19.0 ± 16.1% of fibres, predominantly in the small-diameter fibres. Perivascular cell invasion was also present in one patient.